MASTER THESIS

Compensation of residual field from hollow electron lens asymmetries in the Large Hadron Collider

Author:
Milica Rakić

Mentors:
Dr. Pascal Hermes
Prof. Dr. Mike Seidel

July, 2022

CERN-THESIS-2022-366
00/07/2022

Contents

Abstract

The Large Hadron Collider (LHC) is currently the largest hadron collider in the world. It consists of a 27-kilometre ring, filled with superconducting magnets and beams stored in two separate beam pipes. The accelerator houses four main experiments; ATLAS, CMS, ALICE and LHCb, installed in four beam interaction/collision points. Within the LHC, two beams consisting of 2808 bunches each and around 1.2×10^{11} protons per bunch, are accelerated up to top energy of 7 TeV and peak luminosity of $\sim 2 \times 10^{34}\,\mathrm{cm}^{-2}\,\mathrm{s}^{-1}$.

Tiny fractions of the circulating beam particles lost in the LHC hardware can cause severe damage. Therefore, the LHC is equipped with a sophisticated collimation system, composed of more than 100 collimators that intercept particles at large amplitudes which risk to be in the LHC hardware otherwise. With the upcoming LHC upgrade towards High Luminosity LHC (HL-LHC), the peak luminosity is intended to raise to $5 \times 10^{34}\,\mathrm{cm}^{-2}\,\mathrm{s}^{-1}$, such that the integrity of the collimation system itself is at risk if key devices in HL-LHC would fail.

In particular, particles at large transverse amplitudes are threatening the machine availability and safety, which is why it is desirable to remove them selectively from the beam core, while particles at small amplitudes should be kept to produce the luminosity at the experiments. Hollow electron lenses (HEL) are devices that are going to be installed in HL-LHC to serve this purpose. They create a hollow shaped electron beam that is moving co-axially and inversely directed to the circulating hadron beam. The hollow shape of the electron beam causes particles at large transverse amplitudes to become unstable, while particles in the beam core should stay unaffected. Given the importance for safe operation of HL-LHC, the HELs were included in the baseline of HL-LHC.

However, in real operation, the electron beam is not perfectly symmetric, which results in the existence of electromagnetic fields, creating, in first order, a small dipolar kick acting on the beam core. If no measures are taken to counteract, this residual kick might lead to an increase of the beam dimensions, with detrimental effects on the LHC physics program. This effect could be inhibited by employing the transverse damper (ADT) and inducing a deterministic compensating dipolar kick at each turn the HEL is switched on. This approach might have an impact on the halo depletion efficiency, as well as on the beam core population, which must be understood in simulations.

To explore these questions, tracking tool `XSuite` – a `Python` framework used to simulate particle motion in the beam line elements of particle accelerators – was used and adapted. In this work, the physical figures of merit for the implementation and testing of different operational ADT-HEL approaches in the simulation framework, were derived. The results were used to draw conclusions on the effect of possible ADT compensation schemes on the halo depletion and the particle density in the beam core (and how the latter affects the LHC luminosity). These results deliver an important input on the choice of the final compensation scheme to be applied in HL-LHC.

1 Introduction

The Standard Model of particle physics is a theory describing elementary particles, their fundamental interactions and three of four known fundamental forces - electromagnetic, weak nuclear and strong nuclear force. This model has shown to be theoretically and experimentally self-consistent, however, with some shortcomings. The Standard Model describes only the visible matter, which contributes to only 5% of the universe. It does not explain dark matter – accounting to about 25% of the universe, and dark energy – accounting to remaining 70%. Another shortcoming of the Standard Model is the absence of description of gravity. Therefore, high energy experiments which are probing the smallest of matter, such as the LHC, are essential for understanding and formulating an exact physical description of nature.

The LHC is a storage ring capable of storing hadron particle beams. In a case of the LHC storing proton beams, each beam consist of 2808 bunches storing 1.2×10^{11} protons per bunch. The observed profiles of these bunches are Gaussian with "thick tails". This means that bunches have tails that differ from the ones of a normal distribution, and they are found to be more populated than Gaussian ones (Fig. 1) [11]. Due to the shape of these profiles, fast failure scenarios such as orbit jitters[1] can cause sudden particle losses. These scenarios are dangerous as lost particles can end up hitting magnets and causing magnet quenches, or lead to high enough instabilities that result in beam dumping. To prevent lost particles from causing serious damage, a protection mechanism called the collimation system is implemented in the machine. The collimator system intercepts particles at large betatron and momentum offsets, and disposes of them in a non-damaging manner. Nevertheless, beam tail particles characterising the beam halo population, present a serious threat to the efficient operation of the machine.

In order to increase the potential for future discoveries, and breach the current limitations of the Standard Model, the LHC is preparing for a third upgrade, called High Luminosity LHC (HL-LHC). This upgrade aims to double the beam current and increase the luminosity five times, while reducing the beam emittance by more than 30%. For the system to achieve these envisioned results, it is necessary to understand how the highly-populated beam halos and related loss mechanisms scale with an increase of energy, which is not a priory evident.

As an initial estimate, and to better grasp the source of the problem, lets take into account that current LHC measurements estimate that around 5% of the beam energy is stored in the bunch tails. Assuming linear scaling of this value with energy, the HL-LHC would carry around 35 MJ in beams tails. This value is equivalent to 9.72 kW h, which is enough energy to power all electronics of a single household for a day[2]. Therefore, control of this amount of energy which can be unintentionally deposited across the machine, has to be carefully handled.

[1] Orbit jitters – any effect that causes beam deviation from reference orbit. Not betatron oscillation.

[2] Estimated from average UK electricity consumption: url.

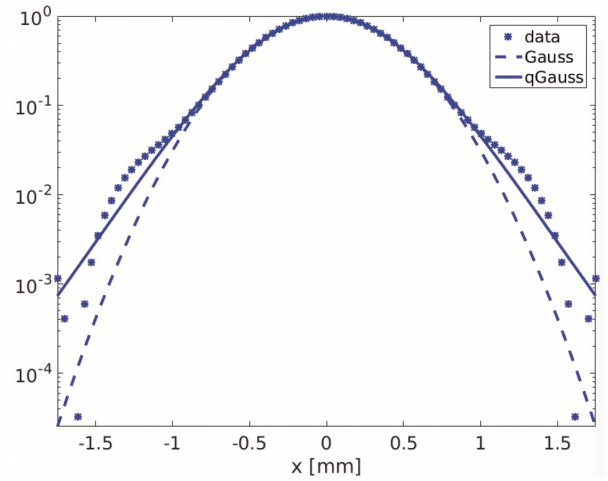

Figure 1: Horizontal bunch profile at flat top energy as measured is presented in blue stars. It is fitted with two functions: the Gaussian (dashed line) and a Gaussian with thick tails (solid line). Image source: [11].

Because of the total energy increase that is expected to be stored in the beam halo once the HL-LHC upgrade is finished, the current collimation system could be put at the limit of its operational capacity. Therefore, to ensure that the machine protection systems are kept operational, the beam halos need to be depopulated in an active and controlled way. The Hollow Electron Lens (HEL) is a device which is planned to be implemented in the HL-LHC with the aim of reducing the circulating beam halo population. The HEL generates a co-axially moving hollow electron beam, that acts only on the particles in the halo, directing them closer to the collimation system, while leaving the beam core unperturbed. Like this, the hollow electrons serve to promote halo particles diffusion speed, supplying small kick to the beam at each turn.

2 The LHC layout

As was previously introduced, the LHC is a storage ring capable of storing hadron beams. This machine is located inside an underground circular tunnel 27 km long in circumference, at and average depth of 100 m. The schematic layout of the LHC ring is shown in Fig. 2. Following the LHC upgrade to the HL-LHC this scheme will be preserved, with certain upgrades to the interaction regions (IR) around interaction points (IP) 1 and 5. [8]

The collider has an eight-fold symmetry with eight straight sections and eight arcs. Four of eight straight sections contain interaction points where the circulating beams are collided and their reaction products recorded. Exactly at these points the four main experiments are located: ATLAS at IR1, ALICE at IR2, CMS at IR5, and LHCb at IR8. The counter-rotating beam 1 (B1, blue) and beam 2 (B2, red), are respectively injected at IR2 and IR8. At IR3 and IR7 the beams are collimated for their momentum and betatron offsets. At IR4 the Radio-Frequency (RF) system is located, and at IR6 the beam dumping system is located. The HEL is planned to be implemented in the IR4.

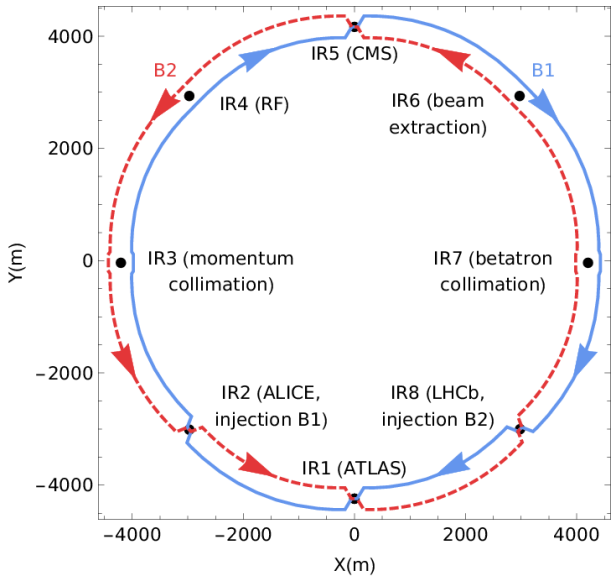

Figure 2: The schematic layout of the LHC ring. The two beams are brought into collision at the four straight sections, IR - 1, 2, 5 and 8. The counter-rotating beam 1 (blue) and beam 2 (red), are respectively injected at IR2 and IR8. IR4 besides housing the RF system, will also contain the HEL. Image source: [1].

3 The LHC collimation system

The collimation system is a set of devices, scattering materials and absorbers, designed to dispose of beam particles at large transverse amplitudes, otherwise referred to as the primary beam halo. Circulating beams have much destructive potential and they can be dangerous for the machine if their energy is wrongfully deposited within it, this is the reason why the particles at large amplitudes – ones closest to interacting with the machine elements – need to be removed. For the purpose of protecting the LHC machine from the beam halo, the beam collimation systems, momentum and betatron offset collimation, are located at two of eight straight segments, as explained in Chapter 2.

The current collimation scheme has been able to successfully operate with populated beam halos, however, it is a question if the same can be assumed for the conditions at HL-LHC with higher beam energies. As previously introduced, the HL-LHC is designed to store around 35 MJ in the beam halo [14], which is above 3 RMS beam sizes and very close to the primary collimators. This amount of energy has significant potential for destruction in the case of orbit jitters, which is one possible initiators of a failure scenario for the HL-LHC. Therefore, to be resistant to orbit jitters, and secure the operation of HL-LHC, it is of high importance to deplete the overpopulated halo. As a part of the halo mitigation system, the Hollow Electron Lens (HEL) is intended to direct halo particles towards the collimation system in a controlled manner in which these particles are disposed of. This operating mechanism is presented in Fig.3.

The particles from the circulating beam halo first reach a co-axially moving hollow electron beam, which gives them a slight transversal kick, in order of 0.1 µrad at every passage. This kick serves to increase the phase space volume covered by the particle, meaning that the particle will reach larger amplitudes. Thereafter, the particles undergo several processes leading to scattering and momentum loss in the collimation system. The primary collimators intercept the beam particles at large amplitudes or momentum offsets, and a series of secondary collimators and shower absorbers remove them from the circulating beam, which is the standard collimation cleaning process. Since the kick that HEL deposits on beam halo particles is in the order of 0.1 µrad, the single-turn effects of HEL are almost negligible. Because the effect of HEL is slow, and significant only in the context of many turn analysis, it can be installed at any position in the ring. Nonetheless, there are reasons why some positions might be preferential over others, and they will be discussed in the following chapters.

3.1 Electron beam generation and characteristics

The hollow electron beam is generated by an electron gun. The gun is directed at an annular thermionic cathode which releases electrons [10, 14]. Once generated these electrons are accelerated by a 15 kV voltage and focused by a set of superconducting magnets. A superconducting solenoid guides the electron beam co-axially over a distance of a few meters. The electron beam is ejected by another solenoid and then dissipated at a collector [12]. The hollow electron distribution is characterised by inner radius (r_1) and outer radius (r_2), between

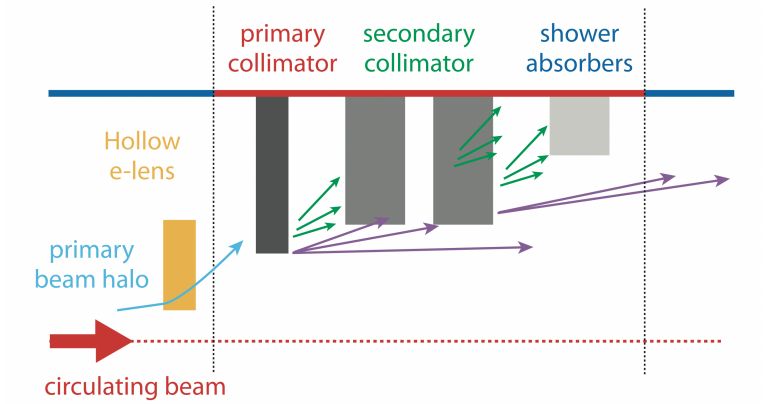

Figure 3: Scheme of conceptual HEL integration in the current collimation system. Image source: [15].

which the electrons are located, as shown on the left in Fig. 4. In an ideally symmetric electron distribution, due to the Gauss law[3], the electric field acting on the particles with amplitudes smaller than r_1 would be equal to zero. All particles with amplitudes larger than r_1 receive a kick in the transverse plane. The size and shape of the electron beam are defined by the cathode shape, cathode state of wear and by all magnets influencing the beam. The dimension of the minimum inner radius r_1 of electron beam is defined by a condition that HEL should not perturb core particles while also strongly affecting particles at amplitudes close to primary collimators [14].

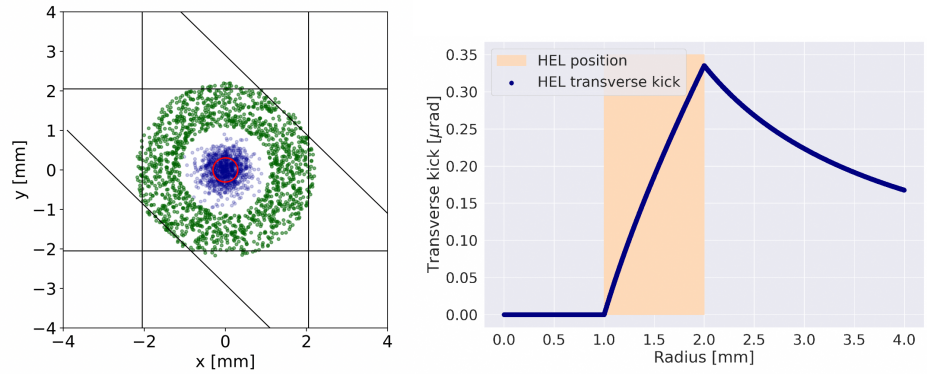

Figure 4: Left – Transverse distribution of the hollow electron beam (green) and the hadron beam (blue) at the HEL. The black lines indicate the cut generated by the primary collimators. The red circle corresponds to one RMS beam size. Image source: [4]. Right – HEL transverse kick as a function of the radial coordinate, plotted in blue. The position of HEL is marked as an orange box.

Electrical fields generated by HEL can be computed by solving the Poisson

[3]Gauss law – the electric field of an arbitrary closed surface is proportional to the electric charge enclosed by the surface.

equation with assigned Dirichlet boundary conditions defined by beam pipe geometry. The obtained electrostatic fields are integrated over straight segments where the HEL acts, giving integrated potential. An estimate of the HEL kick exhausted on the circulating beam is obtained by derivation of this potential [16]. In this way, the problem can be numerically simulated and solved. The transverse kick $\theta(r)$ experienced by circulating beam particles at a distance $r = \sqrt{x^2 + y^2}$ from the circulating beam axis, with assumed constant radial electron current density, is given as [10, 13, 14]:

$$\theta(r) = \frac{1}{4\pi\epsilon_0} \frac{2L_e I_e (1 \pm \beta_e \beta_p)}{\beta_e \beta_p c^2 (B \cdot \rho)_p r} \begin{cases} 0 & \text{if } r < r_1, \\ \frac{r^2 - r_1^2}{r_2^2 - r_1^2} & \text{if } r_1 < r < r_2, \\ 1 & \text{if } r > r_2. \end{cases} \tag{1}$$

where L_e is the effective electron-proton beam overlap region length, I_e is the total electron current, β_e and β_p are electron and proton relativistic betas, $(B \cdot \rho)_p$ is the magnetic rigidity of the proton beam, and r_1 and r_2 are the inner and outer electron beam radius. The "+" sign applies when the co-axially moving electron beam is moving in the opposite direction of the circulating beam, while the "-" sign applies when the electron beam is moving in the same direction as the circulating beam.

Ideally, the electron beam (e-beam) is perfectly symmetrical so that it only acts on halo particles with amplitudes above r_1 and leaves core particles unperturbed. Therefore, in the first case of equation (1), the absolute kick is zero for all radial coordinates smaller than the inner electron beam radius. The second case of equation (1) describes the increase of the kick strength through the e-beam – particles that differ more from the beam core are pushed more substantially to the collimation system. Finally, the third case describes the decreasing kick strength for particles at transverse amplitudes greater than the outer e-beam radius. The described profile of HEL kick as a function of the particle radial distance from the circulating beam axis is shown in Fig. 4 on the right.

Finally, in the previous description and when considering the $r < r_1$ case of equation (1), it was assumed that the electron beam is perfectly symmetrical. Due to many origins of external noise, such as the cathode wear with time and magnetic field defects, and as with every technical device, perfection cannot be reached. This is the reason why the electron beam in reality is expected to be non-symmetrical. This asymmetry will cause the internal electrical field within the r_1 radius to increase to a non-zero value, and therefore, the circulating beam core particles will experience a finite kick. As defined in the HEL design specifications [4], this residual kick should not exceed 1.0 nrad. The effect on the beam dynamics of this residual kick strongly depends on the way the HEL is operated, and is acceptable when the HEL is used in the DC but not in pulsed operational mode, as will be described in the following section.

3.2 Pulsing schemes

The HEL current powering scheme is the primary defining parameter of the shape of the electron beam. To increase the efficiency of the halo depletion, the HEL can be operated in different current pulsing schemes. The efficiency is quantified as the percentage of halo particles removed in a given time frame. Specified target for depletion performance is defined as removing 90% of the primary halo within 5 min of HEL operation [4]. The electron beam can be switched on and off following different patterns on a turn-by-turn basis. There are four basic patterns that have been previously considered [10, 14]:

- Continuous (DC) pattern – the electron beam is turned on at every turn, with fixed current value.
- Pulsed (P_j^i) pattern – the electron beam is turned on for i turns and off for j turns.
- Random (R_p) pattern – the electron beam is switched on/off at each turn randomly, with probability $p \in (0, 1)$.
- Random current (R_I) – the electron beam is switched on at every turn, but the beam current is randomly varied within range $I_e \in (0, 5)$A.

Graphical presentations of listed pulsing patterns are shown in Fig. 5. Due to the complexity of needed hardware upgrades, the random current pattern R_I is the most challenging to realise in the machine. Therefore, it should be utilised only if no other patterns fulfill the needed requirements. Furthermore, all considered pulsing schemes need to fulfill the goal of depleting halo particles as fast as possible without negatively affecting the beam core.

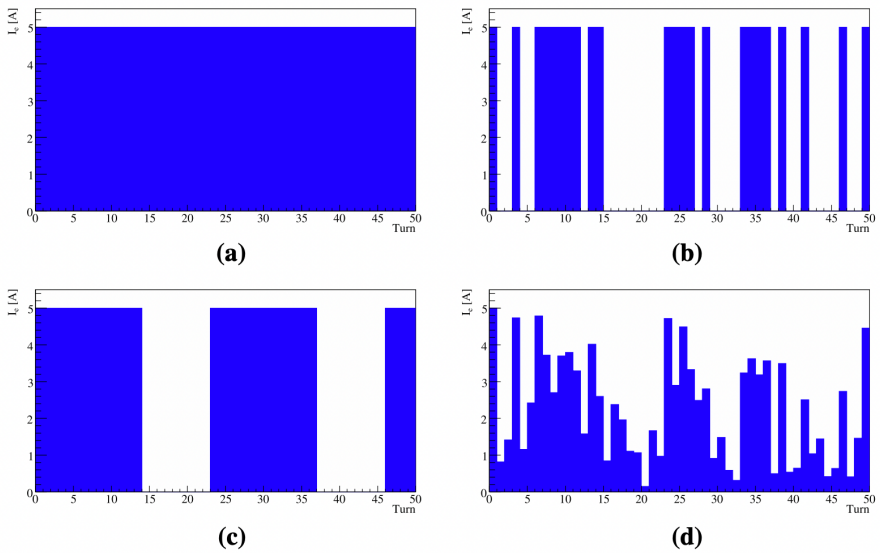

Figure 5: Graphical representation of the four different pulsing schemes; in a – DC pattern, b – pulsed pattern, c – random pulsing pattern and d – random current pattern. Image source: [10].

Previous research [10, 14] has studied halo depletion using these different pulses: DC, P_9^{14}, $R_{0.5}$ and R_I. From the results shown in Fig. 6a, we can see that the DC pulse that gives a constant kick to the beam, turn after turn, is too inefficient. On the other hand, this pulse is also expected to influence the beam core the least, as it generates a constant kick in time. As compared to DC, the deterministic pulsing pattern P_9^{14} gives much better results. The expected performance for random current R_I, can be compared to the random pattern $R_{0.5}$ at operational current of $I = 3\,\mathrm{A}$. Given that the R_I is hardest to accomplish from the hardware point of view, and having in mind this result, there might not be any well-argued need to use this pattern. Finally, the best scheme in terms of halo removal is the random pulsing $R_{0.5}$, with fixed current. For this reason, the random pulsing scheme is further considered in the scope of this thesis.

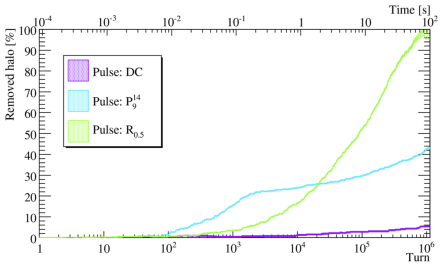

(a) Estimate of the expected beam halo removal after 100 s for various HEL pulsing patterns.

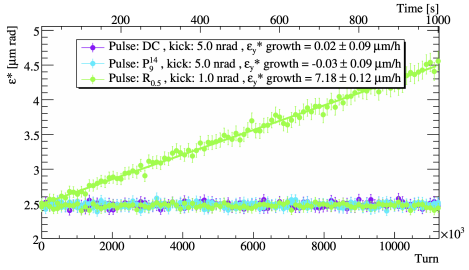

(b) Emittance evolution as a function of turns, plotted for different HEL pulses.

Figure 6: Impact of different pulsing schemes on the beam properties. Images source: [10].

However, one major drawback to the random pulsing pattern $R_{0.5}$ is that it causes an emittance blow-up far beyond the accepted limits. We know from the previous chapter that there is a maximal acceptable limit to the residual kick of 1.0 nrad. The random pulsing pattern induces random kicks that act as noise on the beam core, and cause core particle diffusion to larger amplitudes, effectively increasing the root mean square (RMS) beam emittance. Any increase in the beam emittance limits the achievable luminosity, and therefore, should be avoided.

The results presented in Fig. 6b show the expected emittance growth using different pulsing schemes. No emittance growth is found for both DC and two pulsed patterns. However, the random pattern produces an evident emittance growth. In previous research [9], attempts were made to define an acceptable limit to the emittance growth, accepting value of $0.05\,\mu\mathrm{m\,h^{-1}}$ as a figure of merit. Ultimately, the previously introduced maximal residual kick of 1.0 nrad that is based on stability considerations [2], can be used. Therefore, even though the random pulsing produces fastest halo scraping, and is therefore the most preferred method when considering the preservation of the LHC machine time, it also induces an additional kick to the beam core that needs to be corrected.

To mitigate this emittance growth a transverse damper in feedback mode was planned to be utilised, as will be described in the following chapter.

3.3 Transverse Damper

The transverse damper (ADT) is a device already present in the LHC, used to stabilise the beam against the coupled bunch instabilities caused by high beam intensities and damp unwanted transverse oscillations using a feedback signal. Furthermore, it can be used to apply white noise to induce beam loss for the abort gap cleaning, loss map measurements etc. Therefore, ADT is a very versatile device that can be utilised to damp the beam emittance growth produced by HEL by producing a counter acting kick to the circulating beam, called the compensating kick. To be able to rapidly mitigate any beam orbit deviations due to the residual kick, the ADT can be positioned close to the HEL.

For the purpose of compensating the residual kick from HEL, the ADT can be operated in two modes:

1. Feedback mode – the circulating beam offset is measured by Beam Position Monitors (BPMs) located throughout the machine and fed back to the ADT system, which can then produce a sufficient compensating kick.

2. Deterministic mode – the amplitude of the compensating kick is estimated beforehand based on the phase space conditions that apply at the positions of both the HEL and ADT, as will be shown. The ADT is turned on at every turn the HEL is turned on, and on active turns applies an deterministic kick to the circulating beam.

The feedback mode considers using the already present ADT feedback system – the beam would receive the residual kick from HEL which would offset the beam from reference orbit. This offset would be measured by BPMs downstream of the beam, and fed back to the ADT device. Then the ADT would produce a compensating kick and apply it to the beam. A major problem with this approach is that during the time needed to calculate the offset and the corresponding compensating kick, the beam will have traversed several turns in the machine. Therefore, instabilities caused by the HEL residual kick will have several turns to build up and cause significant beam orbit oscillation.

An alternative approach is to couple the ADT with HEL in a deterministic mode. Every turn that the HEL is switched on the ADT is activated as well. This way the compensating kick by ADT is applied right after the residual kick is produced by the HEL, without any delay. Because the HEL and ADT are not located in the exact same position in the machine, the beam particles will change position in phase space between the positions of HEL and ADT, as shown in Fig. 7. Therefore, the find the ADT compensating kick, the HEL residual kick needs to be scaled for this motion. The needed transformation can be obtained by solving the Hill's differential equation that describes a motion with periodic focusing proprieties [17]:

$$y^{''}(s) + K(s)y(s) = 0. \tag{2}$$

where y is a variable of motion, and $K(s)$ is a position dependant periodic function. The general solutions to the Hill's equation, expressed in a form of a pseudo-harmonic oscillator as given by Courant and Snyder [3], is given by the following set of equations:

$$y(s) = \sqrt{\epsilon\beta(s)}\cos\left(\phi(s) + \phi_0\right) \tag{3}$$

$$y^{'}(s) = -\sqrt{\frac{\epsilon}{\beta(s)}}\Big(\alpha(s)\cos\left(\phi(s) + \phi_0\right) + \sin\left(\phi(s) + \phi_0\right)\Big). \tag{4}$$

where ϵ and ϕ_0 are integration constant determined by the initial conditions, $\beta(s)$ is the periodic betatron amplitude function (or β function), s is path length along the machine and $\phi(s)$ is the phase advance between initial and s position. Because we are interested in estimating kick strengths, we will search for the $\Delta y^{'}$ at point s, needed to compensate for $\Delta y^{'}$ at initial position. By extracting phase terms from equation (4), new phase space coordinates $\bar{y}$ and $\bar{y}^{'}$, called normalised coordinates are defined:

$$\bar{y}^{'}(s) = \sqrt{\beta}y^{'}(s) + \frac{\alpha}{\sqrt{\beta}}y(s). \tag{5}$$

The general transfer matrix for normalised coordinates is a rotation matrix, where the rotation angle is defined by phase advance [3, 17]. Therefore, the transformation of normalised $\bar{y}^{'}$ coordinate is given by:

$$\bar{y}^{'}_s = -\sin\left(\Delta\phi\right)\cdot\bar{y}_0 + \cos\left(\Delta\phi\right)\cdot\bar{y}^{'}_0. \tag{6}$$

where subscript 0 refers to the values at initial position – corresponding to the position of HEL, and subscript s to the values at position s – corresponding to the position of ADT. Therefore, the kicks that HEL and ADT individually give obtained from equation (5) are:

$$\Delta\bar{y}^{'}_{HEL} = \sqrt{\beta_{HEL}}\cdot\Delta y^{'}_{HEL} + \frac{\alpha_{HEL}}{\sqrt{\beta_{HEL}}}\cdot\Delta y_{HEL} \tag{7}$$

$$\Delta\bar{y}^{'}_{ADT} = \sqrt{\beta_{ADT}}\cdot\Delta y^{'}_{ADT} + \frac{\alpha_{ADT}}{\sqrt{\beta_{ADT}}}\cdot\Delta y_{ADT}. \tag{8}$$

Taking into account that the ADT delivers a kick only in $y^{'}$, and assuming the same for the HEL, then $\Delta y_{ADT} = \Delta y_{HEL} = 0$. To find the best ADT kick for compensating the HEL kick we want the ADT kick to have exactly the opposite effect of the HEL kick. Therefore, keeping in mind that to do this the ADT kick needs to be scaled for phase advance as in equation (6), we have:

$$\Delta\bar{y}^{'}_{ADT} = -\cos\left(\Delta\phi\right)\cdot\Delta\bar{y}^{'}_{HEL}. \tag{9}$$

Moving now back to the physical coordinates, we obtain:

$$\sqrt{\beta_{ADT}}\cdot\Delta y^{'}_{ADT} \overset{(8)}{=} -\cos\left(\Delta\phi\right)\cdot\sqrt{\beta_{HEL}}\cdot\Delta y^{'}_{HEL} \tag{10}$$

$$\Delta y^{'}_{ADT} = -\sqrt{\frac{\beta_{HEL}}{\beta_{ADT}}}\cos\left(\Delta\phi\right)\cdot\Delta y^{'}_{HEL}. \tag{11}$$

Finally, the label $\Delta y^{'}$ is changed to θ to match the convention of previous research. Therefore, the calculated ADT kick corrected for phase advance ($\Delta\phi$) is:

$$\theta_{ADT} = -\theta^{r}_{HEL}\sqrt{\frac{\beta_{HEL}}{\beta_{ADT}}}\cos\left(\Delta\phi\right). \tag{12}$$

where θ_{ADT} and θ^{r}_{HEL} are respectively ADT and HEL kicks, and β_{ADT} and β_{HEL} are their respective β functions. One advantage of this approach is that the beam stability is impacted less as the problem is compensated locally and instabilities induced by the residual kick cannot propagate in the machine. Furthermore, because of the direct compensation, potential larger residual kicks on the beam core can be tolerated. The acceptable residual kick from beam stability considerations roughly scales with the square root of the obtained emittance growth with and without the deterministic compensation. This functionality might be important when dealing with any HEL time-related performance degradation, such as the cathode wear with time. In the most efficient system, both of these modes could be implemented and run in parallel. Therefore, both of these approaches must be explored in simulation.

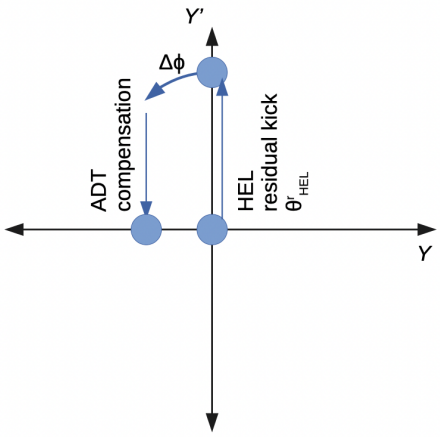

Figure 7: Movement of the circulating beam as represented by a large blue dot, in phase space, between HEL and ADT locations. Axes Y and Y' represent normalised transverse phase space coordinates. Image source: [5].

4 Thesis goals

As was introduced in previous chapters, highly populated beam halos present a threat for HL-LHC and they need to be actively controlled. The HELs are studied for this purpose, however their most effective powering scheme risks to affect the beam core. A strategy using the coupling of the HEL in random pulsing mode and the ADT in either feedback or deterministic mode, was presented. The latter strategy has a drawback in the form of the a priori unknown residual kick, that needs to be determined and compensated, so that the beam emittance growth is controlled while the beam halo is depopulated. The strength of the HEL residual kick is obtained from the characterization of the HEL that will be done before the installation. However, it is essential to confirm that this is still the case after the installation of the lens. Therefore, this needs to be checked in the commissioning.

The goal of this thesis is to find a reliable and efficient commissioning strategy because the HEL residual kick is not known. This strategy needs to be capable to estimate the value of ADT compensation as precisely as possible. To achieve this, the general strategy of this project is to scan over different ADT kick values and find the one which produces the smallest emittance growth – matching the optimal compensating value. The details of the scanning procedure is explained in the following chapter.

Finally, the thesis aims at answering the following questions:

- Can the ADT scan be performed successfully with a single bunch, or are multiple bunches needed?
- What is the optimal sequence of scanning the ADT kick values?
- How robust is this strategy to the introduction of the noise on the HEL residual kick?

The answers to these questions are presented in the following chapters.

5 Simulation setup

The simulations of beam dynamics in the LHC were setup using `Xsuite` [7] framework. The `Xsuite`, and its sub-package `XTrack`, are a collection of python packages needed for the simulation of beam dynamics in particle accelerators. This framework is a successor of previously used `SixTrack` code [6] – single particle 6D symplectic tracking code optimized for long term tracking in high energy rings. The `SixTrack` is mainly used in the LHC for dynamic aperture studies, tune optimization, and collimation studies.

The present scripts in `XTrack` included the integration of the HEL in the LHC sequence, with option for choosing its multiple pulsing patterns. These initial script also included the programming of HEL residual kick. As an expansion of these scripts, during this thesis, the feature of ADT-HEL coupling and optional noise level to the HEL residual kick was implemented in the scripts. The simulation codes were run on CERN batch service HTCondor, using graphic processing units (GPUs). For the purpose of this thesis, all simulation results have been analysed using `python 3.0` programming language.

The impact of ADT-HEL coupling for the goal of efficient halo removal with controlled emittance growth was studied. The ADT was modelled by the deterministic operational mode. In this mode, the HEL is turned on every turn with 50% probability, following the $R_{0.5}$ random pulsing scheme. Every turn that the HEL is turned on, the ADT is turned on as well, and it delivers a kick of constant value in the range from -5.0 to 5.0 nrad. The emittance is recorded every turn, and after the duration of 10 s the ADT kick value is changed to the next value in the given range. From the obtained emittance measurements, the data is fitted to obtain the minimum value, from which the optimal compensating ADT kick is evaluated. The data points are fitted using `python 3.0` `scipy` package, and its function `curve fit` which uses a non-linear least square method to fit the user defined function to a data-set.

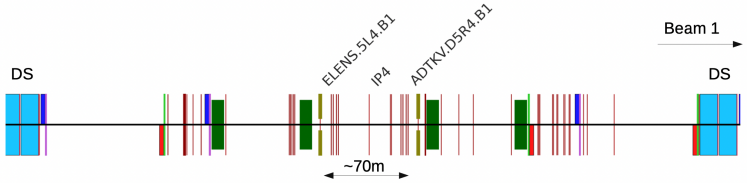

Figure 8: Scheme of the LHC IP4, with marked position of HEL (ELENS.5L4.B1) and ADT (ADTKV.D5R4.B1) The distance between two elements is shown to be around 70 m. Image source: [5].

5.1 The LHC sequence, HEL and ADT parameters

For all studies shown in this thesis, the optics of the HL-LHC V1.5 flat top machine sequence were used. The 'flat top' marker suggests that the optics are used for the configuration after the energy ramp but before squeezing the beams for collisions, at the energy of 7.0 TeV, with $\beta^* = 1$ m in IP1 and IP5, $\beta^* = 10$ m in IP2 and $\beta^* = 1.5$ m in IP8. The studies were done at flat top

because that's the operational condition at which HEL will be used. However, it could also be studied if the HEL residual kick can be calibrated at injection energy which would save a lot of time because the beams wouldn't have to be accelerated. The HEL and ADT elements used for simulations are located in the insertion region 4 (IR4), as shown in Fig. 8. The ADT consists of multiple dampers, that can act in vertical or horizontal transverse plane. From them, the ADTKV.D5R4.B1, was chosen to act on beam one (B1). In reality, it is possible to use both vertical dampers.

The HEL is positioned at a distance $s^* = 3292\,\text{m}$ from IP3 ($s^* = 9957\,\text{m}$ from IP1), and therefore, it is located in IP4. The inner r_1 and outer r_2 radius of the electron beam are set to: $r_1 = 1.4382 \times 10^{-3}\,\text{m}$ and $r_2 = 2.8764 \times 10^{-3}\,\text{m}$ (double the r_1). The electron beam inner radius corresponds to 4.7σ, providing 2σ clearance with respect to the TCP's positioned at 6.7σ. Length of HEL is set to 3 m, the current (when turned on) is set to 5 A and the voltage supplied to the cathode is 10 kV. The ADT is positioned at $s^* = 3364\,\text{m}$ form IP3 ($s^* = 10\,029\,\text{m}$ from IP1), around 70 m downstream of HEL, located at IP4. The beta functions $\beta_{x,y}$ and phase advance $\phi_{x,y}$ of both ADT and HEL are presented in Table 1.

Element	β_x[m]	β_y[m]	ϕ_x[rad]	ϕ_y[rad]
HEL	280	280	7.53	6.78
ADT	213	336	7.58	6.82

Table 1: Optics in transverse plane of HEL and ADT at the position of IP4.

Implementation of HEL in `XTrack` includes the electron beam shape imperfections effects via the residual kick on the circulating beam core. The HEL residual kick is assumed to be constant across the circulating beam core, in the order of a few nano radians, and dipolar. All higher order non-linearities of the system are not inspected. In the same manner, the ADT compensating kick is taken to be dipolar. Furthermore, the studied models do not include the errors emerging from electron beam offset with respect to the circulating beam axis. In all following simulations the center of the HEL is perfectly aligned with the center of the circulating beam.

5.2 Proton distribution parameters

As presented in Chapter 1 of this thesis, the proton beam distribution is not exactly a perfect Gaussian. For the purpose of the studies on total emittance growth and optimal HEL residual kick compensations schemes, the beam distribution was taken to be Gaussian because of simpler process of emittance matching than with a double-Gaussian. The Gaussian distribution is sampled from HL-LHC design emittance of 2.5 µm. The double-Gaussian differs from the Gaussian distribution mainly in the particle population in the distribution tails which is more populated as compared to a ordinary Gaussian distribution. The beam profiles in transverse plane for both Gaussian and double-Gaussian profiles are presented in Fig. 9.

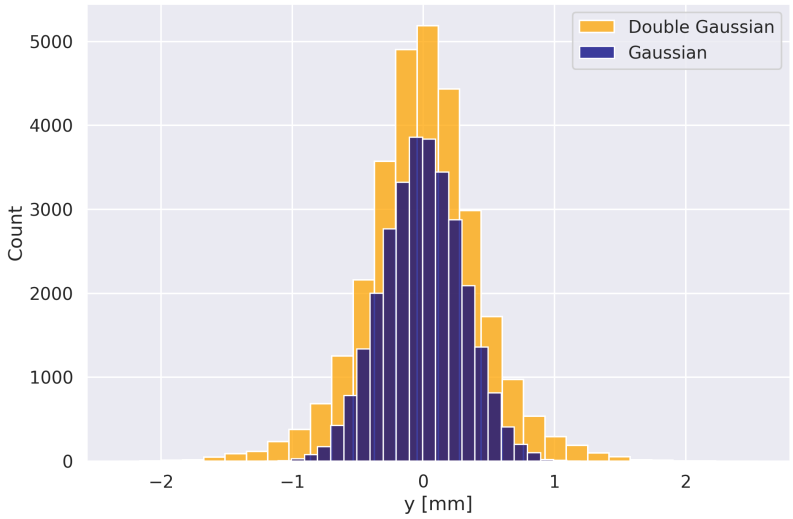

Figure 9: Gaussian (navy colour) and double-Gaussian (orange colour) profiles of the circulating beam in transverse plane.

6 Simulation results

The deterministic mode simulations apply a local compensation of the HEL residual kick, compensating immediately. In the simulations, the proton beam is circulating through the HEL of constant residual kick, set at 1 nrad at every turn. After 112 452 beam turns, which amounts to 10 s in machine time, the emittance of the circulating beam is measured. At the end of every emittance measurement, the ADT kick is changed. This procedure continues until all ADT kicks in the range from -5.0 to 5.0 nrad are sampled. The sampling step size is unique for each study, and is taken to be either 0.25 nrad or 1.0 nrad. The minimal emittance growth inferred from the measured points corresponds to the optimal ADT compensating kick, which would provide the best compensation of the residual kick. To obtain it the emittance values are fitted using the quadratic regression, and from this fit, the minimum is estimated.

To examine the possibility of compensating the HEL residual kick in this way, two approaches – differing by complexity and the amount of LHC machine time they would take – were considered. First approach considers that at the start of every new ADT kick value, the bunches have initial emittance in transverse plane that matches the beam emittance of $\epsilon_0 = 2.5\,\mu\text{m}$. The initial particle distribution is the same for each step. Therefore, the history of the previous ADT kick influence is disregarded, and the simulation behaves as if it is dealing with completely separate bunches at each ADT kick value. This approach was shown to work in previous research [5], but it takes up more bunches to fulfill the measurements. Because this approach has been previously studied, it serves as a good starting point to show the accuracy of the given principle. Because the bunches are the same at the start of each turn, this approach is named the separate bunch scan.

The second approach considers that at the start of every new ADT kick value, the results of all previous kicks are remembered. Therefore, in this case, the starting emittance for each new ADT kick is the final emittance of the previous kick. In this manner, the same bunch can be used for multiple measurements. Therefore, this approach needs fewer bunches to operate. However, as will be shown in the following chapters, this comes at a price of increasing the emittance to really large values, for which there are limitations. Because the same bunches are re-used, this approach is named the single bunch scan. The purpose of introducing the second scanning approach is to explore two extreme cases and what limitations would be faced with them.

6.1 Separate bunches

To estimate the optimal ADT kick using separate bunches, the HEL is setup in the simulation to deliver the residual kick of 1 nrad in the vertical plane and 0 nrad in the horizontal plane. Both the HEL and ADT are turned on or off following the randomly generated pulsing pattern $R_{0.5}$, which is the same for all simulations. Hardware-vise, the on/off signal for the HEL is likely to be generated in the ADT hardware, so that the ADT will always know when the HEL is activated (D. Valuch 2022, personal communication). Using equation (12), it is possible to calculate the theoretical value of optimal compensating kick. The

optics that represent input parameters can be calculated from the LHC lattice and are: $\beta_{HEL} = 280.7$, $\beta_{ADT} = 336.4$ and $\Delta\phi = 0.04$ rad. Using these values in the formula we obtain that the value for the theoretically derived optimal ADT kick is -0.913 nrad.

The beam, consisting of 30 000 particles, circulates for 112 452 turns in the machine, corresponding to 10 s. After 10 s the beam emittance is measured and re-set to ϵ_0 by re-loading the initial Gaussian distribution, and the ADT kick is changed to the next value in the step of 0.25 nrad. The results of measured emittance as a function of ADT kick value are plotted in Fig. 10. The emittance is calculated using the RMS of the y coordinate of the distribution of particles. Data is fitted by a quadratic regression (dashed blue line), and the function minimum is estimated from the fit (red cross). The plotted results show that the absolute emittance decreases in the beginning, until it reaches some minimal value, and then in starts to increase. This result is expected because at the beginning of the scan the ADT kick value is overestimated, but as the scan comes closer to the actual HEL residual kick value of 1 nrad, the emittance blow-up decreases. The same reasoning can be applied for the increasing part of the plotted curve. The optimal ADT kick is estimated from the fit minimum at -0.887 nrad. This result shows a discrepancy between the theoretically predicted value and the value estimated by this technique, reflected by a relative error of 2.8%. The recorded discrepancy can be due to the limited statistics of simulation where only 30 000 particles were included, as well as due to measuring a finite number of emittance values that the fit is estimated from. As will be shown, limited statistic strongly influence the results of simulated emittance.

Nonetheless, the presented results confirm that estimating optimal compensation kick with separate bunches is possible, as was explored in previous research [5]. To confirm the good agreement between theory and simulations for a generalised problem of provisional HEL residual kick value, two more scenarios were simulated. The results of applying the HEL residual kick of 0.5 nrad and 2.0 nrad are presented in Fig. 11. The estimated minimums are -0.443 nrad and -1.778 nrad, with respective relative errors of 11.4% and 11.1%. Even though the error of the estimate is significantly larger, the estimate is approximately correct with some differences that still have to be understood, and could likely come from limited statistics.

6.1.1 Sampling studies

Previous results have shown that by using separate bunches and scanning through the ADT kick values it is possible to estimate a optimal compensation kick, within some margin of error. However, an important question is how does this estimate procedure change (for the better or worse) depending on the way the measurement points are sampled. In reality, the number of measured points shouldn't be too large such that the measurement time is minimised, nor should it be too small such that the accuracy is lost. For example, will the estimated emittance fit minimum change if every second emittance point is sampled, e.g. with sample step size of 0.5 nrad instead of 0.25 nrad? Furthermore, in the context of a commissioning scenario, are there approaches that are preferential over

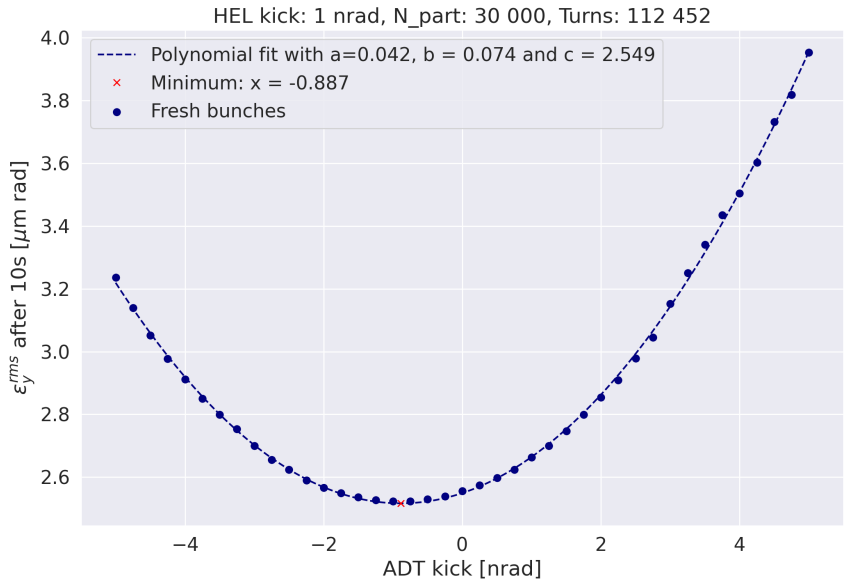

Figure 10: Emittance measurement after 10 s using separate bunches, for different ADT compensation kick values, with 0.25 nrad step size. The data is fitted by a quadratic regression (dashed blue line), with given parameters. From the fit, the minimum is estimated (red cross).

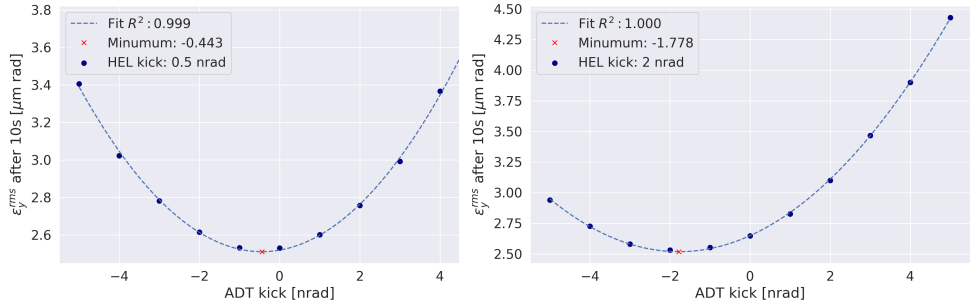

(a) With residual HEL kick of 0.5 nrad. (b) With residual HEL kick of 2.0 nrad.

Figure 11: Emittance measurement after 10 s using separate bunches, for different ADT compensation kick values, with 1.0 nrad step size. The data is fitted by a quadratic regression (dashed blue line), with fit minimum (red cross).

others, and why? In this chapter the influences of different sampling approaches on the measured compensating kick are studied.

Equidistant sub-sampling

For equidistant sub-sampling study the sample presented in Chapter 6.1 is sub-sampled into groups. These groups are generated by recording every n-th point of the original sample, beginning each group with the leftmost point. This sub-sampling scheme can be understood as a change in the sampling frequency of equidistant sampling points. As an illustration, sampling each point corresponds to 0.25 nrad step, every 2^{nd} point to 0.5 nrad step and so on. Each of the sub-samples is fitted by a quadratic regression from which its minimum is estimated. Fitted sub-samples and their minimum estimates are presented in Fig. 12. Each sub-sample is marked by a color and a corresponding number of sampling frequency.

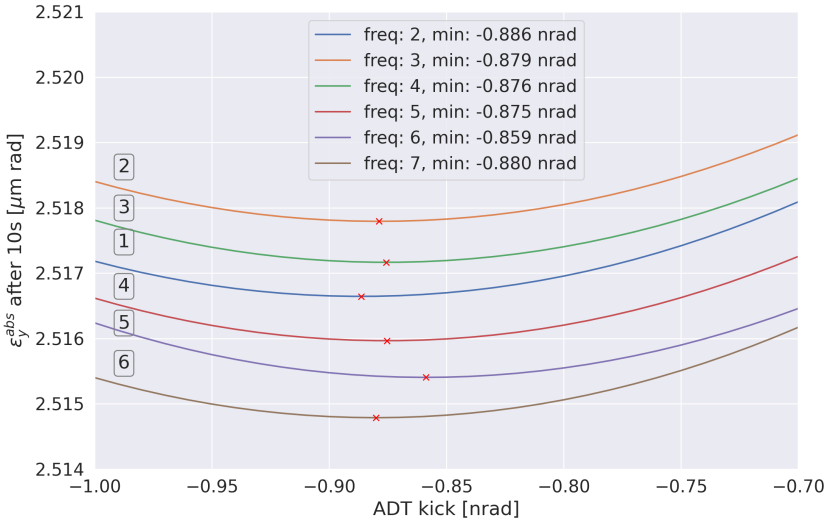

Figure 12: The influence of sub-sampling on the estimated of optimal ADT kick. Each sub-sample is fitted in different colour, and marked in increment numbers.

The presented results show that the estimate of optimal compensating kick doesn't significantly change if every point is sampled or every 2^{nd} point is sampled, with the relative difference between the two of only 0.1%. A bigger difference, albeit still very small, exists if every 3^{rd} point is sampled, with 0.9% relative difference to the full sample. Furthermore, the compensation kick estimate when sampling every 3^{rd} point doesn't significantly worsen. Sampling much less points drastically reduces the density of probed sample. Therefore, even though this sampling scheme doesn't improve the precision of estimating the minimal emittance and the corresponding ADT compensation kick, it does show that there might be no need to sample as densely during run operation. In that way machine time can be spared and potentially used elsewhere.

Continuous sub-sampling

Another interesting aspect regarding separate bunch sampling is whether there is a sub-sampling scheme that produces a more precise estimate. In other words, is there any advantage in scanning ADT kicks in the range from -2.0 to 2.0 nrad for example, over -5.0 to 5.0 nrad range. On the other hand, we can take into account changes in the estimate outcome that may occur when the scanning range is not symmetric to the value of zero. In this study we searched for the optimal ADT kick sub-set from which the compensating kick is estimated with the smallest relative error to the theoretical value of ADT compensating kick. At the beginning of the scan, the subset size is chosen in the range from 4 to the full length of the original data set, of 40 points. Scan is started from the leftmost point of the full data set, to the point corresponding to the subset size. These points are fitted to a quadratic regression (a parabolic function) and the minimum from them is calculated and recorded. Thereafter, the fixed size subset is shifted by one point to the right of the full sample, and the same procedure is continued (as illustrated in Fig. 13). From all these subset positions, the one which produced least error estimate to the theoretical optimal compensation value is selected and recorded. This procedure is repeated again with increasing number of subset points, until the minimal error is determined from all of the scans. As an example, the illustration of scanning with subset with size 4 is shown in Fig. 13. At every step the points within red oval are fitted and error of the minimum is estimated (1^{st} on image), then the red oval is moved to one position to the right (2^{nd} on image) and the procedure is repeated until the final point (n^{th} on image) of the data-set is reached. Thereafter, the sub-sample size is increased and the whole procedure is repeated again.

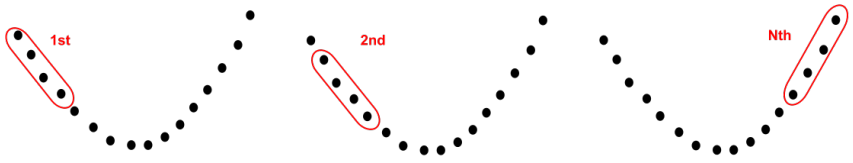

Figure 13: Illustration of continuous sub-sampling procedure for the sub-sample size of four points. At every step the points within red oval are fitted and error of the minimum is estimated (1^{st}), then the red oval is moved to one position to the right (2^{nd}) and the procedure is repeated until the final point (n^{th}) of the data-set is reached. Then, the sub-sample size is increased and the whole procedure is repeated again.

The results of continuous sub-sampling are shown in Fig. 14. The smallest relative error for each subset size is plotted in navy color, and the theoretically estimated value is plotted in red dashed line – corresponding to zero relative error. The original sample is consisted of 40 data points, so to obtain enough data points for fitting, the sampling is scanned in the range of 4 to 40 sub-

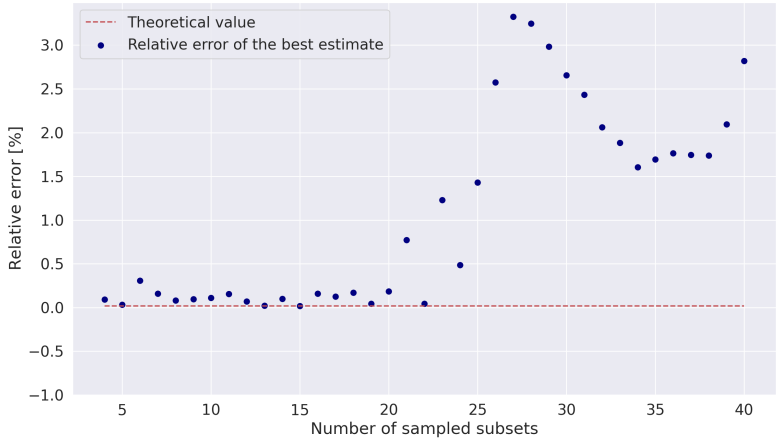

Figure 14: Relative error estimate for sub-samples of different lengths. The best estimate of the relative error for each subset size is plotted in navy color, and the theoretically estimated value is plotted in red dashed line.

sample sizes. These results show that the best estimate for the compensating kick gives a low relative error (less than 1%) for all subsets of 20 or less data points. Once this array grows larger, the relative error increases, up until the value of 27 data point, after which it shows an oscillatory behaviour. Observed trend continues until it finally reaches the error of 2.8% for the complete data set. Possible reason for the increase in the relative error is that once the sub-set size has grown to a certain number of data points, it begins to deviate from the perfect parabola, thus influencing the position of the fit minimum. The very best result is obtained when sampling ADT kick values in the range from -2.0 to 1.5 nrad matching to the subset size of 15 data points, with a kick estimate of -0.912 nrad and relative error of 0.017%. Note should be made that these results are obtained for the original HEL residual kick of 1.0 nrad, and should it change the given optimal ADT kick sub-sample and its respective relative error, will most certainly change too.

This study has shown that it is possible to find a ADT kick sub-sample such that the relative error of the fit minimum of the sub-set is minimised, in relation to the theoretical compensation value. Although showing promising results, this study assumes that the theoretical ADT kick – and therefore the HEL residual kick – is known, which in reality isn't the case. Therefore, even though this approach cannot be utilised in the commissioning scenario, it opens doors for the idea of an alternative scanning scenario. For an instance, assuming that the HEL residual kick shouldn't deteriorate beyond the agreed limit of 1.0 nrad, a gradient descent approach could be performed. The gradient descent scan would allow for point sampling to be less frequent at large ADT kick amplitudes – giving points far from residual kick less weight, and increase in frequency as the kick amplitude is reduced – giving points close to the optimal compensation more weight.

Minimal sampling data set

Finally, there is a question of how many ADT kick samples are needed to have a converging estimate of the compensating kick. In the following study the full data set (comprised of 41 points, ADT kick value in the range from -5.0 to 5.0 nrad, with step size of 0.25 nrad) is separated into subsets. Each subset is composed by randomly choosing a given set of point (re-sampling), starting with 3 points and continuing until the full data set size is reached. Due to the randomness of point choice, chosen points aren't expected to be equidistant. Random choice for the fixed sub-sample size is then repeated 100 more times, to have a set of data points allowing to estimate the variance of the estimated ADT kick for each number of data points sampled. For each subset the compensating kick is calculated by fitting the data to a quadratic regression, and estimating its minimum (procedure as described in previous chapters). The results of such sampling scheme are presented in Fig. 15.

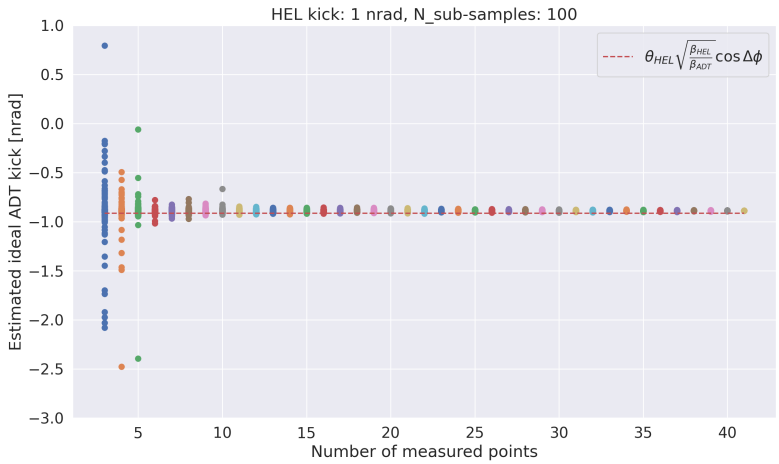

Figure 15: Estimated ADT kick as a function of number of sampled ADT kicks, plotted in coloured dots. The data points used are chosen randomly from the full data set of 41 points. The red dashed line represents the theoretical estimate of the compensating kick.

The presented results demonstrate that for a small number of measured ADT kicks (anything less than 7 points) the estimate for the optimal compensating kick is very dispersed. This is to be expected as the process of random point choosing can select emittances that are far from parabola minimum, and influence the certainty of estimated minimum. As the number of sampled points increase, the dispersiveness is greatly reduced. The estimated compensation kick values start converging to the theoretical compensation kick estimate (presented in the red dashed line in Fig. 15) at around 9 kick samples. Therefore, this study concludes that the minimal value of sampled ADT kicks shouldn't be less than 10 points to ensure a converging estimate of the optimal compensation kick. And although the scenario with the re-sampling can produce constellations

of data points that are not realistic, the comparably extreme study shows that we reliably converge towards a good value if we have 10 points, demonstrating that the method is robust.

6.1.2 Noise studies

Previous research shown in Chapter 6.1 has demonstrated that it is possible to determine the optimal compensating kick by using separate bunches in the case when the HEL residual kick is constant. However, in the real-life scenario due to many sources of the noise, particularly in the HEL subsystems that generate the e-beam, the HEL residual kick may not be constant. Therefore, this study was designed to look into the effect of different residual kick noise levels on the accuracy of the compensating kick estimate. The simulation procedure is exactly the same as described in Chapter 6.1, only this time the HEL kick is changed every turn following the equation:

$$\theta_{HEL} = \theta^0_{HEL} \cdot \left(1 \pm \frac{\Delta_n[\%]}{100}\right). \tag{13}$$

where θ^0_{HEL} is the HEL residual kick without any noise – which is set to 1.0 nrad, and the Δ_n is the noise level in percents sampled from the (0, max. noise level) range, using `python 3.0` package `numpy` and following an uniform distribution. The max. noise level is defined for each simulation and taken to be 0, 1, 5, 10, 20 or 100 %. As an example if the residual kick with no noise is 1.0 nrad and a maximum noise level of 100 % is applied, the residual kick can take any value between 0 nrad and 2.0 nrad. The expectation is that the precision of compensating kick estimate will degrade with increasing levels of noise applied, to a degree which is to be determined. The results of applying different maximal noise levels to the HEL residual kick are shown on Fig. 16 and summarised in Table 2.

Max. noise level [%]	Min. [nrad]	Δ[%]	Δ_t[%]
0	−0.876	0.0	4.1
1	−0.876	0.1	4.0
5	−0.870	0.6	4.7
10	−0.876	0.04	4.1
20	−0.879	0.4	3.7
100	−0.826	5.6	9.5

Table 2: The results of applying different maximal noise levels to the HEL residual kick where: Min. [nrad] is the estimate of the minimum of the fitted quadratic regression (estimate of the compensating kick), Δ[%] is the relative error to the no-noise case, and Δ_t[%] is the relative error to the theoretical compensating kick estimate.

From the presented values we can see that the estimate of the optimal compensating kick doesn't change much (relative change of 5.6%) when no noise is applied and when a noise of 100% is applied to the residual kick. This result in itself wouldn't make much sense were it not for the procedure by which the noise level Δ_n is sampled. As briefly mentioned above, the Δ_n is a randomly

sampled value in a given range from the uniform distribution. Therefore, even though the residual kick can take any value between two limits, after a certain amount of time (or in other words, after many turns in the machine) the effective residual kick will take the value of the sampled distribution mean. Because the mean of the uniform distribution is the median of the sum of its lower and upper limit, for the case of having a 1.0 nrad residual kick with noise level of 100%, this mean value is also 1.0 nrad. Therefore, even though a large noise level is applied, effectively over many turns the approach will find the same kick, corresponding to the mean with the noise.

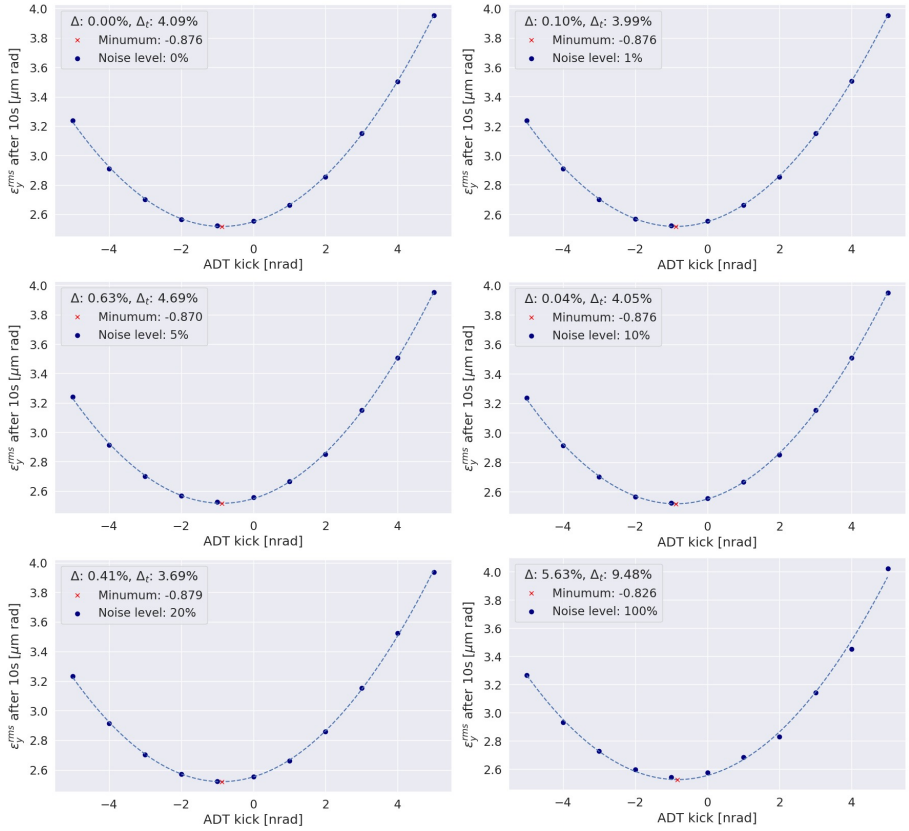

Figure 16: Cumulative emittance after 10 s for different ADT kick values and different maximal noise levels: 0% upper left, 1% upper right, 5% mid left, 10% mid right, 20% bottom left and 100% bottom right.

To test the accuracy of this assumption, the same procedure is repeated when only a positive error is applied. The '±' sign in equation (13) is exchanged to a '+' sign, and the noise is added on top of the HEL kick each turn. If the presented results were due to the sampling from uniform distribution, changing from a symmetric noise to an additive noise should demonstrate a systematic shift in the optimal compensating kick estimate. The results of comparing these two noise application cases are presented in Fig. 17. Cumulative emittance after 10 s as a function of different ADT kicks for symmetrical 100% noise is plotted in red, additive 100% noise in navy and no-noise case in green colour. All three

data sets are fitted to a quadratic regression from which the minimal value is estimated.

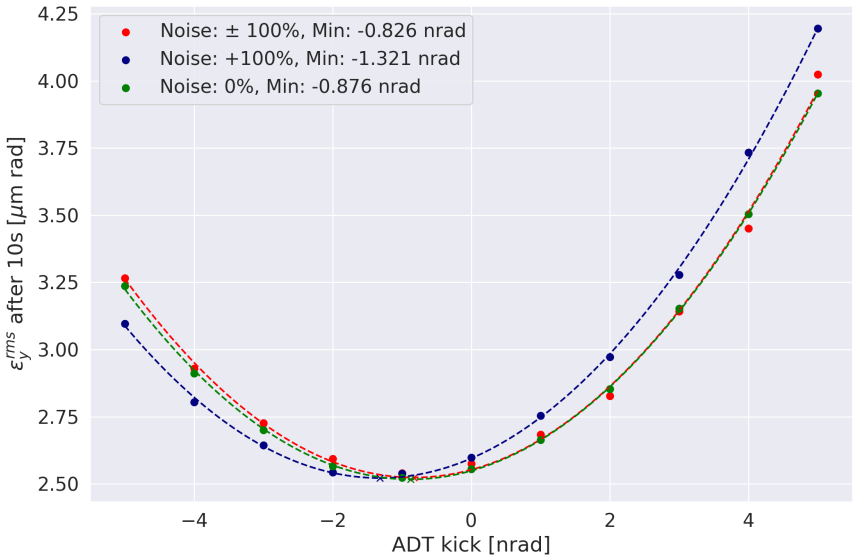

Figure 17: Comparison of cumulative emittance after 10 s for different ADT kick values for three cases: symmetrically applied 100% noise in red, additive applied 100% noise in blue and no-noise applied in green.

There are two main conclusions that can be derived from these results. Firstly, by comparing the compensation estimate of the red and blue plots (symmetrical and additive noise), we can see that the compensation value is shifted from -0.826 nrad to -1.321 nrad, which corresponds to the difference of about 0.5 nrad. Considering how the mean HEL kick for symmetrical 100% noise is 1.0 nrad and for additive 100% noise is 1.5 nrad, this value exactly matches the mean difference of 0.5 nrad, confirming the presented assumption. Secondly, when comparing the red and green plots (symmetrical noise and no-noise case), we can see that they are very similar. Therefore, these two results straighten the above postulated assumption of the influence of sampling from the uniform distribution.

Furthermore, the results of Fig. 17 show that for an additive maximal noise level of 100% on the 1.0 nrad kick, which corresponds to the effective mean kick of 1.5 nrad, the estimated optimal compensating kick is -1.321 nrad. The relative error of this value to the theoretical mean is 3.5%. As compared to the optimal compensation kick estimate with no-noise and separate bunches of 2.8%, we can see that the results are only slightly worse. Therefore, the derived procedure is also suitable in case that the noise applied to the HEL is additive and of significant level, as long as the mean of the residual kick does not change.

However, even thought the compensation is possible with very large noises, it is a question of how effective it will be. For this reason, it is important to look into the cumulative emittance growth after all kick samplings. The reduction factor (RF) is the ratio of the rate of emittance growth with no ADT present and the emittance growth with the simulated noise model, and ADT operated at the estimated ideal deterministic kick. Higher the RF is, the better compensation is given by the ADT. Cumulative emittance growths over 1×10^6 turns are shown in Fig. 18 and fitted to a linear regression model. From these fits, the curve slopes are determined and growth rates calculated. Four different cases are presented; no-noise and no-ADT in blue, symmetrical 100% noise in orange, asymmetrical 100% noise in skyblue, and no-noise and theoretical ADT compensation in red. The calculated RF for no-noise and perfect compensation performs the best, with value of around 21 RF, followed by asymmetrical noise of 3.5 RF and finally symmetrical noise of around 2 RF. These results enforce the postulation that even though the required compensating kick can be well estimated with high levels of symmetrical noise, the quality of compensation is drastically reduced. Therefore, the optimal ADT kick can be well identified even if noise is present, as long as the noise is around a constant mean value. However, these noise values only serve to test the robustness of the applied method to noise as the expected noise levels are much lower than considered in these simulations. Furthermore, when the noise is present, even with the good compensating ADT kick, the emittance growth is larger than in no-noise case. Thus, the consequence of noise is a worse compensation of the emittance growth, but nonetheless the commissioning strategy has shown to still work under these circumstances.

Finally, the shape of RF curve was studied. In Fig. 19 the change of the RF with the increase of symmetrical noise level is shown. The noise level is increased in the steps of 10%, until the 100% value is reached. The results show that even though the ADT compensating kick can be estimated fairly well with high noise levels, the overall ability to reduce the emittance growth decreases with higher noise levels. Therefore, these results yet again strengthen the idea that the ADT should be used by coupling the deterministic and feedback operational mode.

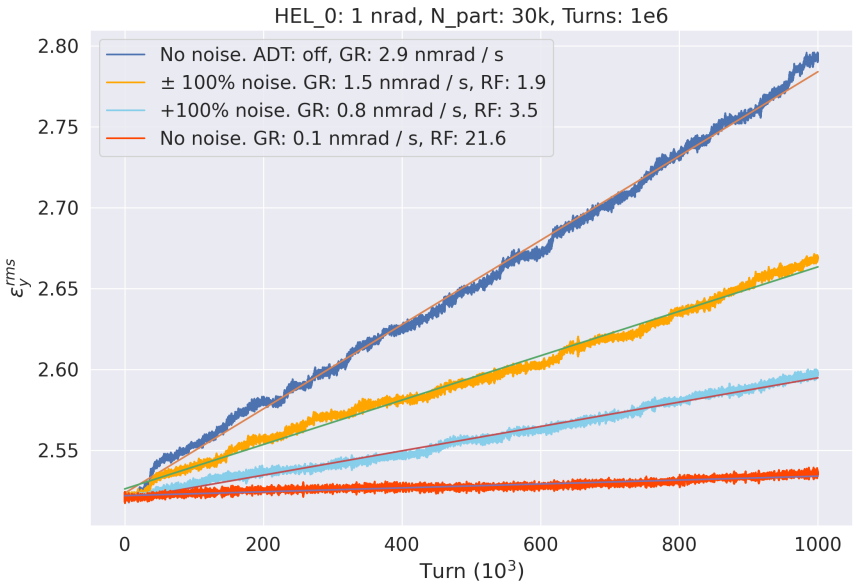

Figure 18: Cumulative emittance after 1×10^6 turns with different operations of ADT: no-noise and no-ADT in blue, symmetrical 100% noise in orange, asymmetrical 100% noise in skyblue, and no-noise and theoretical ADT compensation in red colour. GR stands for emittance growth rate, RF for reduction factor.

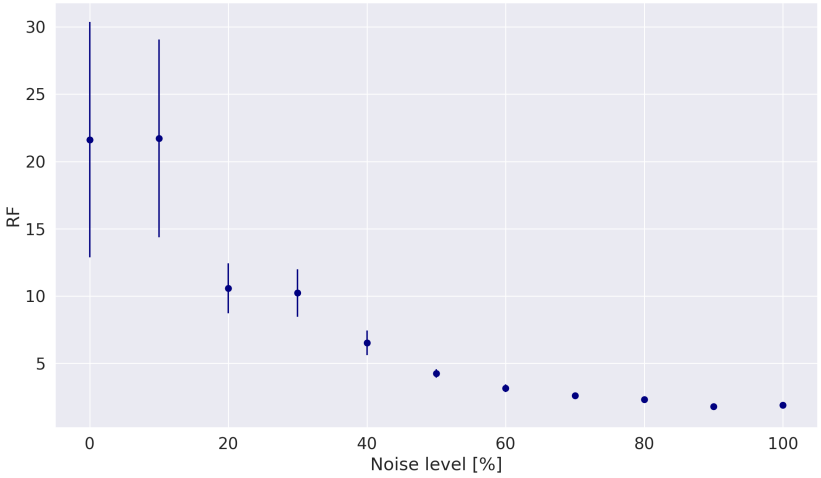

Figure 19: Reduction factor as a function of the level of symmetrically applied noise to the HEL kick, with 1σ standard deviation errors.

6.2 Single bunches

In this chapter the feasibility of using single bunches instead of separate bunches for the goal of faster measurement taking is evaluated. The simulation is setup in a similar manner as explained in Chapter 6.1, with all parameters retaining the same values, and measurement procedure being identical. The ADT kicks are scanned in the range from -5.0 to 5.0 nrad in the steps of 0.25 nrad. The beam emittance is set to $\epsilon_0 = 2.5\,\mu\text{m rad}$ only at the start of the simulation, and it is not re-set at the start of each new ADT kick scan. Therefore, the last emittance measurement of previous simulation is an entry value of the emittance for the following simulation. The results of this approach are presented in Fig. 20, where the cumulative emittance measurement after 10 s of each ADT kick is plotted in navy color.

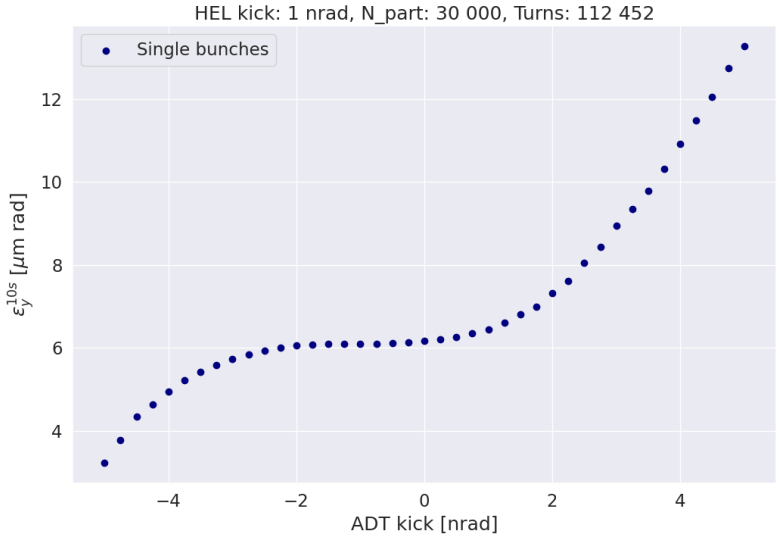

Figure 20: Cumulative emittance measurement in transverse plane after 10 s of each ADT kick is plotted in navy color.

As compared to the separate bunch result in Fig. 10 we can see that the cumulative emittance for single bunches behaves very differently. The emittance initially starts growing when the compensating ADT kick is still far from the HEL residual kick value of 1 nrad. As the compensation kick scan approaches the residual kick, the emittance growth rate per scan step is greatly reduced. This could be expected because the ADT kick is compensating exactly, or 'almost exactly', for the residual kick, so that the net kick on the circulating beam is close to zero. After this stage, when the compensating kick once again over-shoots the residual kick value, the cumulative emittance continues the increasing trend. The final emittance reached via this scanning approach is $\epsilon = 13.3\,\mu\text{m}$, which is around 5.3 times greater than the initial beam size. This result is specific for the step size chosen, and will differ for another step size. The obtained final emittance is so large that particles of the beam will be lost in the collimators

located at 6.7σ, which will be shown in the following results.

The figure of merit for estimating the optimal compensating kick of the ADT is the derivative the curve shown in Fig. 20, as it represents the relative emittance increase per ADT kick step. Therefore, the relative emittance increase from one ADT kick to another is presented on Fig. 21 (bottom plot, scattered blue points). Similarly to the trend observed in Fig. 10 the emittance decreases as the ADT kicks approach the residual kick, and after the ADT kick surpasses it, the emittance increase per scan step starts further increasing. However, at the point of around $3\,\mathrm{nrad}/4 \times 10^6$ turns, the relative emittance deviates from the expected parabolic shape and flattens between $(0.5 - 0.7)\mu\mathrm{m}$ range, as can be seen at the location of right most points of Fig. 21. This result in itself is important as it can be drawn back to an underlying issue that can be experienced when operating such a scanning scheme – particle loss at the collimators.

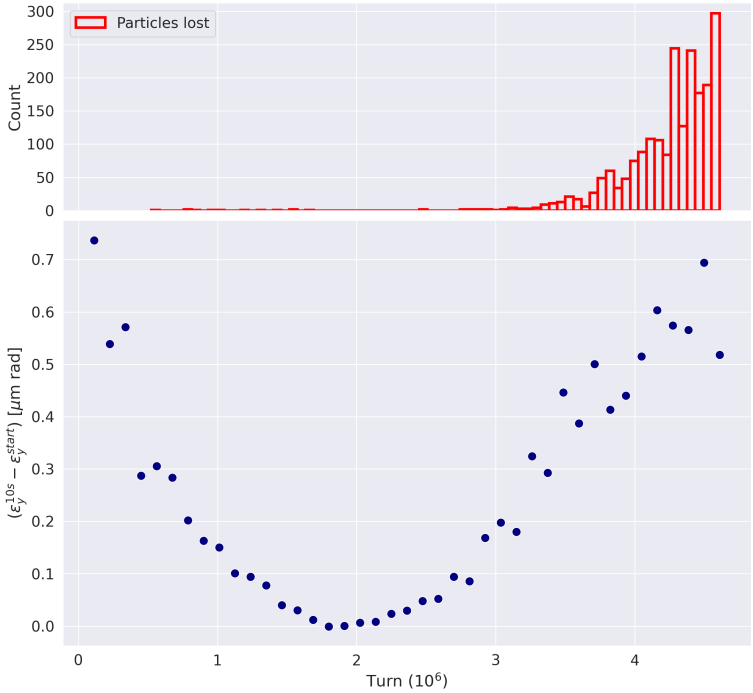

Figure 21: Bottom – absolute emittance difference for single bunches as a function of number of turns in the machine. Top – count of lost particles as a function of the number of turns.

To explain the reason behind this behaviour, we can take a look at Fig. 22, where the different types of influences to the circulating beam generated by the ADT, the HEL and the three primary collimators (TCPs) are shown. The HEL works in the way that it supplies most of the kick to the halo particles that enter the hollow electron beam (dark blue colour, thick black lines), as predicted by equation (1). Due to the asymmetries of the electron beam shape, there is an additional residual kick that the core particles obtain (light blue colour, thin black lines), of much lower strength. On the other hand, the ADT doesn't

distinguish between the halo and core particles, and it delivers a constant kick at the location of the mean charge of the bunch. This means that the ADT acts with same intensity on the bunch as a whole. Therefore, at large ADT kick values, where the compensating kicks are exceeding by far the HEL's residual kick, the beam is driven to large size by the ADT. Once the beam size surpasses the setting of the TCP, located at 6.7σ, the beam particles will get lost in the collimation system. Plotting the number of lost particles per turn, shown on top plot of Fig. 21, confirms that recorded emittance saturation corresponds to particle loss, driven by the above explained mechanism.

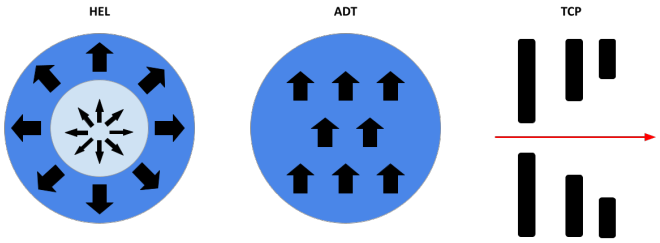

Figure 22: Schematic representation of the HEL, ADT and TCP influence on the beam. The black arrows show the intensity of the electric field strength produced by ADT/HEL at a given point in the beam, while the blue hue color grade show the intensity of the kick given to the beam. The rightmost image shows the TCP jaws in black, and the direction of beam traversing it in red.

These results show that it is very important how the ADT kicks are scanned for the commissioning scenario, where there should not be any particle losses originating from this compensation system. Using a single bunch imposes a limitation to the number of steps that can be sampled, otherwise the beam will touch the collimators and be lost. Evidently, scanning the ADT compensation kicks in 0.25 nrad steps, starting at -5 nrad and finishing at 5 nrad produces too much of an emittance growth. These results bring forward two important questions. Firstly, is it necessary to scan the values of the ADT kicks with given density of 0.25 nrad step size – how does increasing the step size affect the best estimate of compensation kick and the fit precision? Secondly, is there an alternative scanning scheme that would reduce the cumulative emittance growth at the end of the scanning procedure?

To address these questions, a few different scanning schemes were looked into. These inspected schemes are defined as follows:

1. Consecutive – the ADT kicks are scanned consecutively from the -5.0 nrad value to the 5.0 nrad in 1.0 nrad steps.

2. Outer to inner – the ADT kicks are scanned in a outer to inner scheme given by the following array: $[0, -5, 5, -4, 4, -3, 3, -2, 2, -1, 1]$ nrad.

3. Inner to outer – the ADT kicks are scanned in an inner to outer scheme given by the following array: $[0, -1, 1, -2, 2, -3, 3, -4, 4, -5, 5]$ nrad. This

scheme takes an inverse scanning order compared to the outer to inner scan.

The graphic illustration of the three ADT kick scanning approaches: consecutive, outer to inner and inner to outer scheme, respectively, are shown on Fig. 23. The black dots represent the emittance measurements for each ADT kick, illustrating simulation measurements. The red arrows show the direction and order in which the ADT kicks are sampled. The obtained results of these three approaches are further described and presented in the following sections.

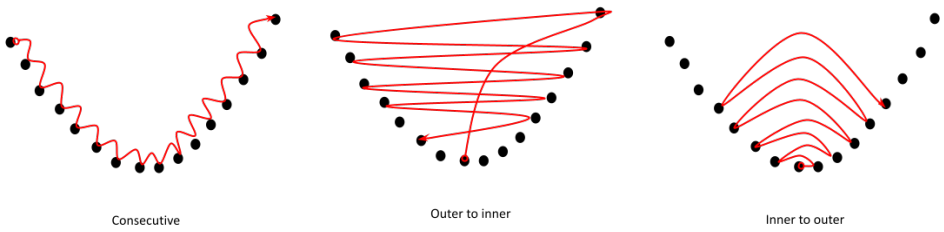

Figure 23: Graphic illustration of the three ADT kick scanning approaches: consecutive, outer to inner and inner to outer scheme, respectively. The black dots represent the emittance measurements for each ADT kick, and the red arrows show the direction and order in which the ADT kicks are sampled.

6.2.1 Consecutive scanning scheme

Results presented in the last chapter show that when the ADT kicks are sampled consequently in the steps of 0.25 nrad the final emittance is five-fold greater than the initial emittance. This can present a problem as particles hit TCPs and are lost in the machine, driving the beam intensity loss. Therefore, to prevent this from happening the total emittance growth needs to be limited. A way of reducing the total emittance growth is to sample less ADT kick values, which can be accomplished by increasing the sampling step size. In this study, the step size is increased from 0.25 nrad to 1.0 nrad, reducing number of sampling points, and consequently reducing the time the beam is exposed to these invasive compensation kicks by one fourth. The ADT kicks are still sampled in the -5.0 to 5.0 nrad range, as the specification of the residual kick is 1.0 nrad, this range should likely be covering the real residual kick.

The results of this scanning scheme are shown in Fig. 24a, and compared to the consecutive scanning scheme with 0.25 nrad step size. Consecutive scanning scheme with 0.25 nrad step size is denoted as a dense scan, and scanning scheme with 1.0 nrad step size is denoted as a light scan. The image shows the relative emittance measurement as a function of ADT kick value for the consecutive dense (navy colour) and consecutive light (orange colour) scanning schemes. The light scheme data points are fitted to a quadratic regression, shown in dashed orange line. The best estimate for the ADT kick from this fit is -0.801 nrad, with relative error of 12%. Comparing this result with the value obtained with separate bunches of -0.887 nrad, with relative error of 2.8%, it is evident that there is yet another discrepancy between obtained results. The results obtained with single bunches are therefore less precise.

On the other hand, compared to the consecutive dense scanning scheme, with light scheme the occurrence of emittance saturation at large ADT kicks is no longer present. The emittance continues its polynomial rise, as is expected, to its final value of $\epsilon = 6.35\,\mu$m, only 2.5 times larger than ϵ_0. Therefore, just by increasing the step size of ADT scan values, the final emittance was reduced twofold. To confirm that this light scan removes the issue of particle loss at the collimators, the particle loss for light scan (orange colour) is plotted against particle loss for dense scan (navy colour), on Fig. 24b. We can see that the large particle loss recorded starting at turn 3×10^6, has been removed, and therefore the particles are not being lost due to the emittance blowup induced by the ADT. These results are significant as they show that fist of all, single bunches can be used instead of separate bunches to estimate the value of the best compensating ADT kick, and second of all, that a good estimate can be made with less scanning point and therefore, less machine time.

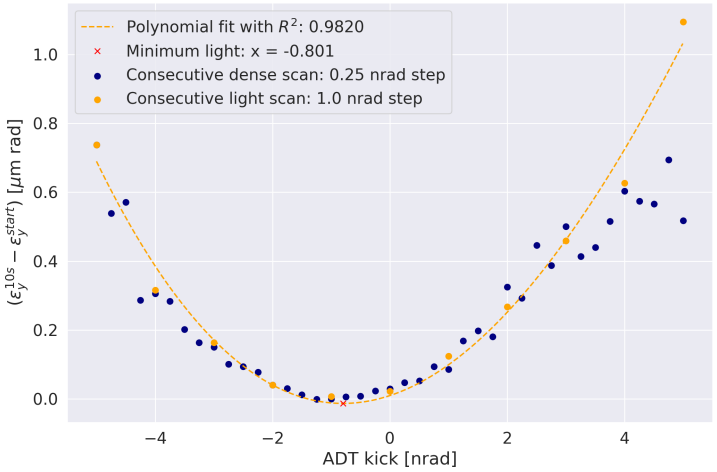

(a) Absolute emittance difference as a function of ADT kick value for consecutive dense (navy colour) and consecutive light (orange colour) scanning schemes. The consecutive light data points are fitted to a quadratic regression, shown in dashed orange line. The consecutive dense data points are shown only for comparison.

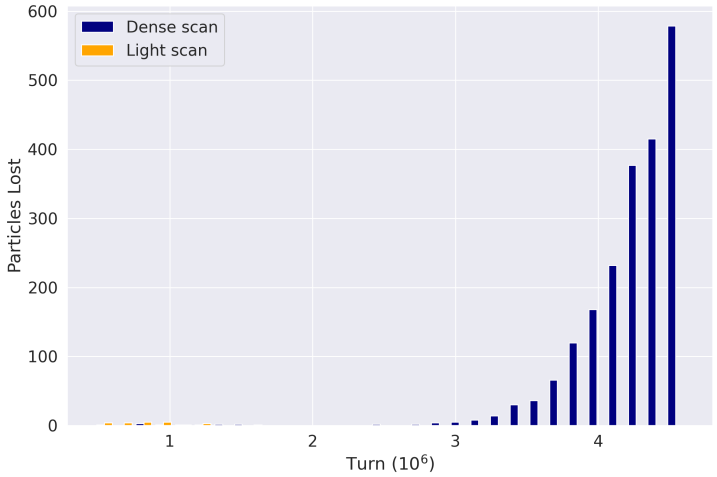

(b) Particle loss detected on collimators as a function of total turns for consecutive dense (navy colour) and consecutive light (orange colour) scanning schemes.

Figure 24: Influence of the consecutive dense and light scanning schemes on the relative emittance measurement and particle loss on the collimation system.

6.2.2 Outer to inner scanning scheme

Another approach aimed to reduce the total emittance growth is the outer to inner ADT kick scan scheme. This scheme starts scanning at zero ADT kick and continues by applying symmetrical (to the zero value) values of positive and negative kicks, starting at the value of 5.0 nrad and continuing to smaller values in the steps of 1.0 nrad. Motivation for constructing such scheme is to see how the history of the scan changes the final emittance, when each applied kick is compensated by its counterpart of opposite sign after the duration of 10 s.

The results of this scanning scheme are presented in Fig. 25 and compared to the consecutive light scanning scheme. Measured relative emittance after 10 s of each ADT kick value for outer to inner scanning scheme is plotted in orange colour, and for the consecutive light scheme in navy colour. Both data sets have the same scanning step size of 1.0 nrad. Both data sets are fitted as presented by dashed orange and navy lines. The given fits aren't constant for the hole bunch and they wont give a final fixed error estimate, initial particle distribution sampling set will influence the error measurement. From this fit the compensating kick is estimated at -0.810 nrad, with relative error of 11% to the theoretically predicted value. We can see that even though the outer to inner scan gives somewhat better estimate of the kick, it doesn't drastically change the emittance growth, with the final emittance value of 6.59 µm. Therefore, even though this scheme can be used, it doesn't prove to be very advantageous to the consecutive light scheme.

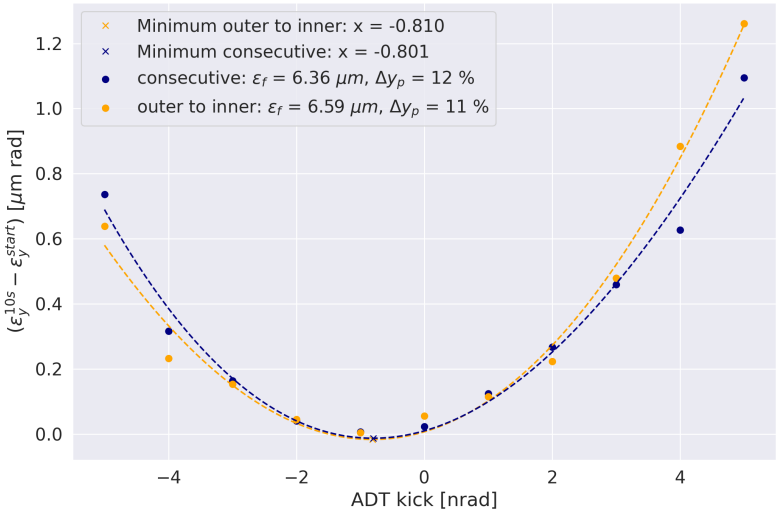

Figure 25: Absolute emittance difference as a function of ADT kick value for consecutive light (navy colour) and outer to inner (orange colour) scanning schemes. Both data sets are fitted to a quadratic regression, presented in dashed blue and orange lines. Minima of both fits are represented as orange and navy crosses.

6.2.3 Inner to outer scanning scheme

The final scanning pattern that was examined resembles the outer to inner scheme, and can be interpreted as its inverse. The ADT kick value scan starts at zero value and continues symmetrically outwards in 1.0 nrad step size, until the value of 5.0 nrad is reached. One big advantage of this approach is that the ADT kick history is recorded starting at smaller values – where we expect the HEL residual kick to be, and ends at large values. Due to this history construct, when analysing the results in the post-processing stage, large ADT amplitudes can be discarded one-by-one to estimate their influence on the data fit and compensation kick estimate.

The results of this scanning scheme are presented in Fig. 26 in green colour, and compared to the outer to inner (red colour) and consecutive light (blue colour) scanning schemes. Measured relative emittance after 10 s is plotted as a function of ADT kick value. Same as with the consecutive and outer to inner scans, the inner to outer scan points are fitted to a quadratic regression, shown in dashed green line. Compensating kick is estimated from fit at -1.013 nrad, with relative error of 11%, same as with the outer to inner scan. Furthermore, the total emittance growth for inner to outer scheme is much better as compared to the previous schemes, with final emittance value of 6.28 µm. The presented results show that these scheme can be utilised, however, it still under-performs when compared to separate bunch scanning scheme.

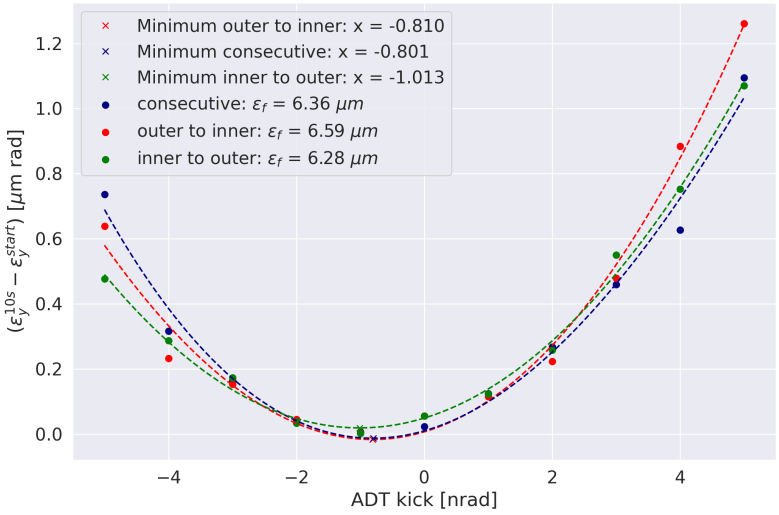

Figure 26: Absolute emittance difference as a function of ADT kick value for inner to outer (green colour), consecutive light (navy colour) and outer to inner (red colour) scanning schemes. All data sets are fitted to a quadratic regression, presented in dashed green, blue and red lines, respectively. Minima of all fits are represented as crosses of their respective colour.

6.3 Statistical artefacts

Limited statistic, presenting due to the finite number of simulated particles, are an important phenomenon influencing simulation results. Because the computing time of simulations needs to be finite, and optimally as short as possible, there is a need to limit the number of particles that are being simulated. However, because the beam consist of around 1×10^{11} particles per bunch, to represent the physical reality enough particles are needed. To evaluate the impact of limited number of simulated particles on the emittance spread, three separate simulations with different number of particles were preformed. The emittance is measured and recorded at each turn over one thousand turns. Finally, the recorded emittance is plotted as a histogram for each simulation to illustrate the emittance spread.

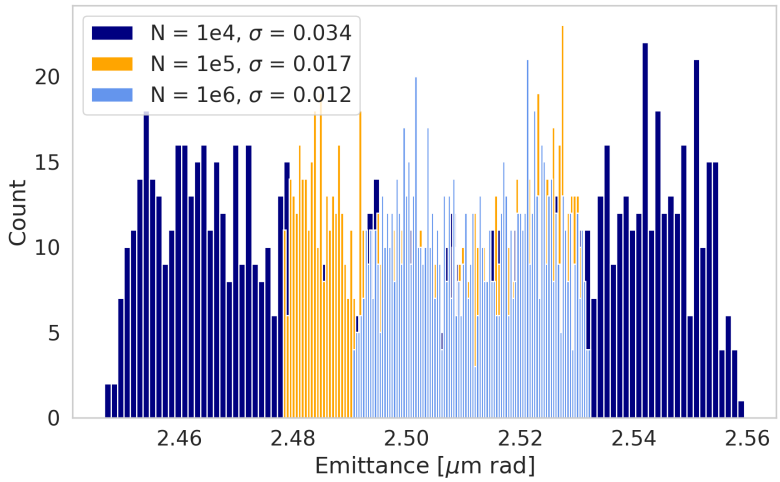

Figure 27: Influence of number of simulated particles on the emittance spread. In navy plot 1×10^4 particles, in orange 1×10^5 and in light blue 1×10^6 particles.

An example of limited statistics impact on the measured emittance spread is shown on Fig. 27. Emittance spreads are recorded when the number of simulated particles is 1×10^4, 1×10^5 or 1×10^6, and plotted in navy, orange and light blue colour respectively. These results show that increasing the number of particles decreases the emittance spread, which could be expected. On top of that, standard deviation σ was calculated for all three cases, and is 0.034 for 1×10^4 particles, 0.017 for 1×10^5 particles, and 0.012 for 1×10^6 particles. Therefore, coming from the first to the second case the standard deviation decreases by 50%, and from second to the third by another 29%. What can be concluded from these values is that the simulation results depend highly on the number of simulated particles, and increasing their number helps the precision of the obtained results. However, as the number of simulated particles grows larger, the sensitivity of the results to this growth is decreased.

Furthermore, to be able to obtain trustworthy results and still perform sim-

ulations relatively quickly, the number of particles can be limited if other approaches for statistically significant data collection are undertaken. One of the tactics that was employed for presented studies is an alteration in the way the emittance is calculated. Instead of calculating emittance at each turn, the particle positions are collected over a larger set of turns, and the emittance value is calculated from this extended data-set. The number of collection turns defines the roll value. Therefore, if 3×10^4 particles are simulated with a roll of 10 turns, it would be the same effect as simulating 3×10^5 particles and calculating the emittance at each turn. The effect of the emittance growth is small enough to be negligible over 10 turns, so there is no risk in losing accuracy by implementing this approach.

An example of this approach is shown in Fig. 28, where the beam is simulated with 30 thousand particles, for 112 452 turns, and with 1 nrad HEL residual kick for each ADT compensating kick. The emittance measured with roll equal to one is plotted with blue dots, and emittance with roll equal to ten is plotted in orange dots. Both data sets are fit with a same parabolic function, shown in blue and red lines, respectively. We can see that the blue dots – where emittance is taken every turn – are much more diffused as compared to the orange dots – where the emittance is taken every ten turns. In this way better statistic can be achieved without sacrificing precious computing time.

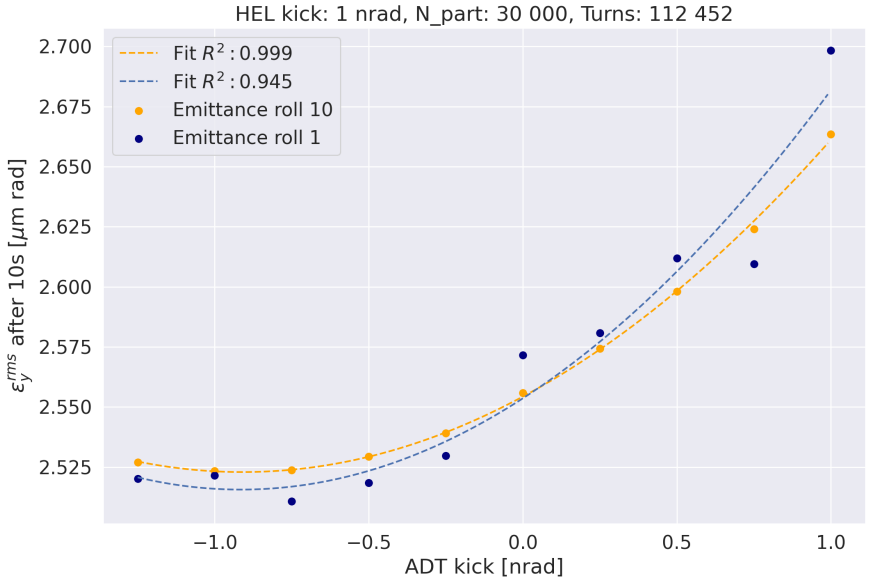

Figure 28: Emittance measurement after 10 s for different ADT compensating kicks, fixed HEL kick of 1 nrad and 112 452 turns for each data sample.

7 Conclusion

The planned upgrade of LHC to the HL-LHC aims at increasing the stored beam energy by the factor of two, which could compromise the integrity of the collimation system as it is. One of critical safety threats are beam particles at large transverse amplitudes, otherwise known as halo particles – that will, if lost very fast, deposit large amounts of energy into the collimation system, thus potentially damage it. The observed bunch profiles in the LHC have shown to have overpopulated halo compared to what one would have with a Gaussian distribution profile, therefore the same is expected for the beams in HL-LHC. To mitigate the risk of fast losses of the highly energetic beam halo from orbit jitters in HL-LHC, the overpopulated halos need to be depopulated. The HELs are devices which are a part of the machine baseline, introduced for the purpose of removing beam halos in a controlled and rapid manner. Previous research [10] has identified that operating the HEL in a random pulsing scheme allows for the fastest halo removal in a given time frame, making this pulsing operation favorable. However, in reality, the electron beam in the HEL cannot be perfectly symmetrical, which produces a residual kick to the circulating beam core particles. This kick, paired with the random pulsing operation, could cause an emittance growth of the beam core, which would be detrimental to the achievable LHC physics goals and possibly trigger instabilities.

As a mitigation measure, to compensate for the detrimental effect of the HEL residual kick, the nearby transverse damper (ADT) can be coupled to the pulsing pattern of the HEL and produce a counteracting kick in the opposite direction. However, for the ADT to be used in this way, the residual kick produced by the HEL, which is a priori unknown, needs to be determined in the commissioning phase before HL-LHC is run, in which the HEL is used.

In this thesis, an operational scheme for experimentally determining the optimal compensating ADT kick has been proposed. It has been demonstrated that the operational compensating kick can be estimated if we have enough time and bunches. The scheme includes scanning the ADT kick values in a certain range, and measuring the respective final emittances of the beam after 10 s and each applied ADT kick. The starting point to the studies is a scenario in which the emittance growth for different compensating ADT kicks is scanned assuming that each data point is recorded with a new bunch at initial emittance of 2.5 µm rad. In this manner, the quadratic regression can be performed on the measured emittance data, and from it, the minimum can be calculated. The estimated kick at which the smallest emittance growth is predicted by the quadratic regression will therefore correspond to the optimal ADT compensation kick. The process of commissioning the ADT compensation is not trivial. The ADT kick sampling density strongly influences the time needed for the commissioning of the HEL-ADT coupling and must be carefully chosen. The presented results have demonstrated that in this scenario the emittance growth can be reduced by a factor of 10 to 21.

Furthermore, the proposed operational scheme has been tested with various hypothetical levels of the HEL residual kick noise. It was shown that the proposed operational scheme is robust even against high levels of noise reaching up

to $\pm 100\%$, and that it is capable of determining the optimal ADT compensating kick even then. However, such high noises would influence the total efficiency of the HEL-ADT deterministic coupling, and lower the quality of the compensation. With 100% symmetrical noise the emittance growth reduction factor is decreased to the value of (1.9 ± 0.2), compared to reduction factor of (21.6 ± 8.7) without noise. Regardless of the fact that given noise levels of $\pm 100\%$ are colossal, unrealistic and not to be expected, these results demonstrate the feasibility of the proposed approach in simulations.

Finally, it was checked if the commissioning can be made more efficient if less bunches are used. The results have demonstrated that the proposed operational scheme is capable of operating with either single or separate bunches. It was shown that single bunches can be used, but at an expense of a slight precision decline when estimating the optimal ADT compensation, as compared to using separate bunches. Therefore, to increase the efficiency, single bunches can be used for the HL-LHC commissioning, especially when taken into account that the feedback system can be utilised.

In conclusion, future studies should include work on operating the ADT in the feedback operational mode, and also in the coupled deterministic and feedback operational mode. Both of these approaches might have an impact on the halo depletion efficiency, as well as on the beam core population, which must be understood in simulations. Nonetheless, the HEL-ADT coupling has shown to be a promising solution for compensating the effect of the HEL residual kick and could become the baseline mode of operation for when the HEL is going to be used.

Acknowledgements

I am extremely grateful to my mentor Pascal Hermes, for his forbearance, kindness and above all, for the immense amount of knowledge he passed on to me. Many thanks to my colleagues from the LHC collimation project team, and most notably Stefano Radaelli for the constructive comments that have significantly improved this master's thesis and undoubtedly raised it to a higher level. I extend my appreciation to Xavier Buffat, Gerd Kotzian, Martin Soderen, and Daniel Valuch for their valuable input on simulations. Numerous thanks to Tatiana Pieloni and Mike Seidel for introducing me to the branch of accelerator physics, as well as for their perpetual guidance and support during my studies. I owe everlasting gratitude to my family and friends, who have always believed in me and provided me with unconditional support.

References

[1] R. Bruce et al. "Reaching record-low beta* at the CERN Large Hadron Collider using a novel scheme of collimator settings and optics". In: *Nuclear Instruments and Methods in Physics Research Section A: Accelerators, Spectrometers, Detectors and Associated Equipment* 848 (Dec. 2016). DOI: 10.1016/j.nima.2016.12.039.

[2] X. Buffat. *Instability latency with the e-lens residual dipole kicks*. Apr. 19, 2021. URL: https://indico.cern.ch/event/1026380/contributions/4309563/attachments/2223502/3775305/2021-04-09_ELensLatency.pdf (visited on 06/27/2022).

[3] E.D. Courant and H.S. Snyder. "Theory of the Alternating-Gradient Synchrotron". In: *Annals of Physics* 281.1 (2000), pp. 360–408. ISSN: 0003-4916. DOI: https://doi.org/10.1006/aphy.2000.6012. URL: https://www.sciencedirect.com/science/article/pii/S0003491600960123.

[4] P. Hermes et al. "HL-LHC Beam Dynamics with Hollow Electron Lenses". In: *JACoW* HB2021 (2022), MOP09. DOI: 10.18429/JACoW-HB2021-MOP09.

[5] P. Hermes, R. Bruce, and X. Buffat. *Compensation of the Hollow Electron Lens residual kick*. Dec. 17, 2021. URL: https://indico.cern.ch/event/1105248/contributions/4653492/attachments/2366514/4041077/211217_ColUSM_HEL_ADT_compensation.pdf (visited on 06/28/2022).

[6] R. De Maria et al. "SixTrack Version 5: Status and New Developments". In: *Proc. 10th International Particle Accelerator Conference (IPAC'19), Melbourne, Australia, 19-24 May 2019* (Melbourne, Australia). International Particle Accelerator Conference 10. https://doi.org/10.18429/JACoW-IPAC2019-WEPTS043. Geneva, Switzerland: JACoW Publishing, 2019, pp. 3200–3203. ISBN: 978-3-95450-208-0. DOI: doi:10.18429/JACoW-IPAC2019-WEPTS043. URL: http://jacow.org/ipac2019/papers/wepts043.pdf.

[7] R. De Maria et al. *XSuite*. https://github.com/xsuite/. 2021.

[8] R. De Maria et al. "High Luminosity LHC Optics and Layout HLLHCV1.4". In: *Journal of Physics: Conference Series* 1350.1 (2019), p. 012001. DOI: 10.1088/1742-6596/1350/1/012001. URL: https://doi.org/10.1088/1742-6596/1350/1/012001.

[9] E. Metral et al. "Update of the HL-LHC operational scenarios for proton operation". In: (2018). URL: https://cds.cern.ch/record/2301292.

[10] D. Mirarchi et al. "Nonlinear dynamics of proton beams with hollow electron lens in the CERN high-luminosity LHC". In: *Eur. Phys. J. Plus* 137 (2021), 7. 28 p. DOI: 10.1140/epjp/s13360-021-02201-5. URL: https://cds.cern.ch/record/2798109.

[11] S. Papadopoulou et al. "Modelling and measurements of bunch profiles at the LHC". In: *J. Phys. Conf. Ser.* 874.1 (2017), p. 012008. DOI: 10.1088/1742-6596/874/1/012008.

[12] D. Perini et al. "Design of high-performance guns for the HL-LHC HEL". In: *JINST* 16 (2021), T03010. 9 p. DOI: 10.1088/1748-0221/16/03/T03010. URL: https://cds.cern.ch/record/2767764.

[13] H. Rafique. "MERLIN for High Luminosity Large Hadron Collider Collimation". In: *Doctoral thesis,* University of Huddersfield (2017).

[14] S. Redaelli et al. "Hollow electron lenses for beam collimation at the High-Luminosity Large Hadron Collider (HL-LHC)". In: *JINST* 16 (2021), P03042. 28 p. DOI: 10.1088/1748-0221/16/03/P03042. URL: https://cds.cern.ch/record/2767761.

[15] S. Redaelli et al. "Plans for deployment of hollow electron lenses at the LHC for enhanced beam collimation". In: (2015), 4 p. URL: https://cds.cern.ch/record/2025002.

[16] G. Stancari. *Calculation of the transverse kicks generated by the bends of a hollow electron lens*. 2014. DOI: 10.48550/ARXIV.1403.6370. URL: https://arxiv.org/abs/1403.6370.

[17] A. Wolski. *Introduction to Beam Dynamics in High-Energy Electron Storage Rings*. 2053-2571. Morgan and Claypool Publishers, 2018. ISBN: 978-1-6817-4989-1. DOI: 10.1088/978-1-6817-4989-1. URL: https://dx.doi.org/10.1088/978-1-6817-4989-1.